Summer 2011

Thermo-physical properties measurement and steel - ceramic shell interactions in investment casting

Chirag Mahimkar

Department:

THERMO-PHYSICAL PROPERTIES MEASUREMENT AND STEEL - CERAMIC SHELL INTERACTIONS IN INVESTMENT CASTING

by

CHIRAG RAJENDRA MAHIMKAR

A THESIS

Presented to the Faculty of the Graduate School of the

MISSOURI UNIVERSITY OF SCIENCE AND TECHNOLOGY

In Partial Fulfillment of the Requirements for the Degree

MASTER OF SCIENCE IN MATERIALS SCIENCE & ENGINEERING

2011

Approved by

Von L. Richards, Advisor
Simon Lekakh
K. Chandrashekhara

ABSTRACT

Investment casting is a process in which a ceramic shell is prepared on a wax or foam pattern. The wax is melted out or the foam is burnt out and the shell is sintered to have sufficient strength to withstand casting conditions. The investment casting process is very important as it produces near net shape castings which reduce the need for subsequent operations of castings like machining etc.

Investment casting shells are subjected to a number of heating cycles during pattern removal, firing, preheating before pouring and finally during solidification. The thermo-physical properties of the shell play an important role during these processes. One focus area of this research was measuring the thermal conductivity and the specific heat capacity of investment casting shells. The measured properties were included in a simulation software database (Magmasoft).

A second focus area of the research was casting surface defects due to liquid steel – ceramic shell interactions. A special cube-shaped specimen with a deep pocket region was designed and simulated using Magmasoft. Three different types of shells were prepared with silica, zircon and alumina flour in the prime coat slurries. For comparison, shells prepared around the same pattern were obtained from three industrial foundries. Shells were preheated to 800°C and poured with HY130 steel. Shell samples in contact with the steel were taken from the pocket region of the castings, polished and SEM/EDS analyzed. Multiple interaction products included complex *Mn-Si-O*, *Al-Si-Mn-O* and *Fe-Si-Mn-Al-O* oxides were experimentally identified. The experimental results are discussed with respect to the thermodynamic predictions. The results can be used for shell material selection and to identify casting procedures that would limit these defects.

ACKNOWLEDGEMENTS

I would like to thank Dr. Von Richards and Dr. Simon Lekakh for their continuous help and support throughout this research. Their guidance had been a great motivational force for me. I also wish to express my gratitude to Dr. K. Chandrashekhara for reviewing this thesis.

I would like to thank U.S. Army Benet Labs for providing funding for research. I acknowledge the support of Steel Founders Society of America and the Investment Casting foundries that participated in this research.

I would like to thank graduate students Matthew Thompson and Gregory Harrington for operating the laser flash equipment. I thank William Peach, Darryl Kline, Wesley Everhart, Daniel Snyder, Andrew O'Loughlin, Abhilash Dash, Arpana Murthy, Anthony Wilshire and Edith Martinez for their help in conducting heats. I thank Jamie Fitzgerald and Tom Towey for their assistance in the sample preparation.

Finally I would like to thank my parents, brother and roommates for their support.

TABLE OF CONTENTS

Page

ABSTRACT iii

ACKNOWLEDGEMENTS iv

LIST OF ILLUSTRATIONS vii

LIST OF TABLES xi

SECTION

1. INTRODUCTION 1

1.1. BACKGROUND 1

1.2. LITERATURE REVIEW 4

1.2.1 Thermo - Physical Properties of Ceramic Shells 4

1.2.2 Metal - Cermic Shell Interactions 10

1.3. FOCUS OF RESEARCH 19

2. EXPERIMENTAL PROCEDURES 21

2.1. SLURRY PREPARATION 21

2.2. PATTERNMAKING 23

2.3. PATTERN COATING 23

2.4 SHELL FIRING 24

2.5 DENSITY MEASUREMENT BY ARCHIMEDES METHOD 24

3. THERMO- PHYSICAL PROPERTIES OF CERAMIC SHELLS 26

3.1. SHELL PREPARATION 27

3.2. LASER FLASH TEST 28

3.3. DIFFERENTIAL SCANNING CALORIMETRY (DSC) 33

3.4. RESULTS 34

3.5. DISCUSSIONS 42

3.6. CONCLUSIONS 50

3.7. FUTURE WORK 50

4. LIQUID STEEL - CERAMIC SHELL INTERACTIONS IN INVESTMENT CASTING 52

4.1 PATTERN DESIGN 53

4.2 MAGMASOFT SIMULATIONS 54
4.3 FACTSAGE MODELING 57
4.4 SHELL PREPARATION 58
4.5 RESULTS 62
4.5.1 Silica Prime Coat Shells 62
4.5.2 Alumina Prime Coat Shells 63
4.5.3 Zircon Prime Coat Shells 63
4.5.4 Industrial shells (Foundry A, B & C) 63
4.6 DISCUSSIONS 70
4.6.1 Thermodynamic predictions 70
4.6.1.1 Factsage first model 70
4.6.1.2 Factsage second model 71
4.6.2 Possible steps involved in liquid steel - prime coat reactions 72
4.6.3 Depth of penetration of interaction products 75
4.7 CONCLUSIONS 77
4.8 RECOMMENDATIONS 77
4.9 AREAS OF FUTURE INTEREST 78
4.9.1 Effect of superheat 78
4.9.2 Effect of inhibitor gas 78
4.9.3 Vacuum induction melting 78
APPENDIX 79
BIBLIOGRAPHY 87
VITA 92

LIST OF ILLUSTRATIONS

Figure Page

2.1 Mixing plate and scraper bar shown with an empty mixing bucket 21

2.2 Brookfield DV-II+ Pro viscometer used to measure slurry viscosity..... 22

3.1 Block diagram of a laser flash system 29

3.2 FLASHLINE ™ 5000 (Anter Corporation) laser flash equipment 31

3.3 Samples and Standard (a) before graphite coating and (b) after graphite coating..... 32

3.4 Shell samples and standard placed in holder before laser flash test 32

3.5 Example of thermal diffusivity measurement of reference and sample 34

3.6 Specific heat capacity of the silica shell prepared at Missouri S&T foundry from the laser flash test (fired at 900°C). 35

3.7 Specifc heat capacity of the silica + zircon shell prepared at Missouri S&T foundry from the laser flash test (fired at 900°C). 36

3.8 Specific heat capacity of the silica + aluminosilicate shell prepared at Missouri S&T foundry from the laser flash test (fired at 900°C). 36

3.9 Specific heat capacity of the shell (fired at 900°C) measured by the laser flash test for foundry A (flour - zircon, stucco - aluminosilicate) 37

3.10 Specific heat capacity of the shell (fired at 900°C) measured by the laser flash test for foundry B (completely fused silica based) 37

3.11 Specific heat capacity of fused silica based shell not fired (Run 1 - first firing, heating of green shell and Run 2 - second heating cycle the same shell)..... 38

3.12 Specific heat capacity of fused silica based shell fired to 800°C (Run 1 - first firing, heating of green shell and Run 2 - second heating cycle the same shell) 38

3.13 Specific heat capacity of fused silica based shell fired to 1200°C (Run 1 - heating cycle of preliminary fired 800°C shell and Run 2 - second heating cycle the same shell) 39

3.14 Thermal conductivity of the silica shell prepared at Missouri S&T foundry (fired at 900°C) by the laser flash test..... 40

3.15 Thermal conductivity of the silica + zircon shell prepared at Missouri S&T foundry (fired at 900°C) by the laser flash test 40

3.16 Thermal conductivity of the silica + aluminosilicate shell prepared at Missouri S&T foundry (fired at 900°C) by the laser flash test 41

3.17 Thermal conductivity of the shells (fired at 900°C) measured for foundry A (flour - zircon, stucco - aluminosilicate) by the laser flash test 41

3.18 Thermal conductivity of the shell (fired at 900°C) measured for foundry B (completely fused silica based) by the laser flash test 42

3.19 Comparison of specific heat capacity data of pure refractory materials obtained from Factsage (fused silica, aluminosilicate- kyanite) with the data obtained from laser flash test for the shells prepared at Missouri S&T fired at 900°C 43

3.20 Comparison of thermal conductivity data of pure refractory materials [33] with the data obtained from laser flash test for the shells prepared at Missouri S&T foundry fired at 900°C 43

3.21 Possible phase transformations [34] in silica shells..... 46

3.22 Presence of cristobalite and tridymite in the shell fired to 1200°C [36]..... 47

3.23 Specific heat capacity database shown in Magmasoft for (a) fused silica based shells (b) silica + zircon based shells (c) silica + aluminosilicate based shells 48

3.24 Thermal conductivity database shown in Magmasoft for (a) fused silica based shells (b) silica + zircon based shells (c) silica + aluminosilicate based shells..... 49

4.1 Reaction product (Mn-Si-O) penetrating inside ceramic shell 53

4.2 Foam patterns 54

4.3 Control points 55

4.4 Cross sectional view of the shell 55

4.5 Temperature distribution at 100% fraction solid steel which shows the internal corners remain at high temperatures 56

4.6 Temperature histories for control points at the corner of the casting and at 0.5(control point 1), 3.5(control point 2), 6 mm(control point 3) from the casting surface inside the ceramic shell during steel solidification 57

4.7 (a) Missouri S&T shells before pouring (b) castings after pouring 60

4.8 Industrial shells: (a) foundry A (b) foundry B (c) foundry C 60

4.9 (a) Shells coated with kaowool and (b) preheating in kiln 61

4.10 Silica prime coat shells interaction products (a) Al-Si-Mn-O and (b) Fe-Si-Mn-O phases 65

4.11 Alumina prime coat shells interaction products (a) Al-Si-Mn-O (b) Fe-Si-Mn-O phases 66

4.12 Zircon prime coat shells interaction products (a) Fe-Zr-O-Si (b) Al-Si-Mn-O. 67

4.13 Interaction products Al-Si-Mn-O (a) and Fe-Si-Mn-O (b) phases observed in shell samples from foundry A 68

4.14 Interaction products Al-Si-Mn-O (a) and Fe-Si-Mn-O (b) phases observed in shell sapmples from foundry B 69

4.15 Interaction products Fe-Si-Mn-O phases obseved in shell from foundry C 70

4.16 Solid phase formation during cooling reoxidation slag (Factsage) 73

4.17 Equilibrium amount of the dissolved prime coat (D) versus initial reactant composition as S/(S+C) at 1550°C 74

4.18 Maximum depth of reaction product location in prime coat of studied shell versus percentage apparent porosity 76

LIST OF TABLES

Table Page

3.1 Compositions of shells prepared at Missouri S&T lab for Cp and K measurement 28

4.1 Investment casting shells prepared at Missouri S&T foundry 59

4.2 Shells obtained from the commercial foundries 59

4.3 Chemistry of HY130 steel in 2 heats poured at Missouri S&T 61

4.4 Equilibrium model prediction for interaction products by Factsage 73

1. INTRODUCTION

1.1. BACKGROUND

The investment casting process has been used widely for the production of small and medium sized precision steel and aluminum castings with complex geometry. Now it is finding many more applications in the fields of military, marine, aerospace etc. There are many design advantages [1] of the investment casting process. Any degree of external complexity as well as wide range of internal complexity can be achieved. Any castable alloy can be used, including ones that are impossible to forge or are too difficult to machine. The absence of parting lines and the elimination of substantial amounts of machining by producing parts very close to final size give investment casting an enormous advantage over sand casting and conventional forging. The long-standing use of investment castings in aircraft engines for the most demanding applications has fully demonstrated their ability to be manufactured to the highest standards.

There are two distinct processes [2] used for making investment casting molds: the ceramic shell process and the solid investment (solid mold) process. The ceramic shell process starts with dipping a foam or wax pattern in slurry made of binder and flour (fused silica, zircon, alumina etc.). Most common binder used today is colloidal silica since the United States government imposed limits on the use of ethyl silicate. The dipped pattern is allowed to drain for sufficient time and then refractory powders (crushed stucco) are applied to the slurry coated pattern. The first coat is called as prime coat and plays a major role in surface finish of the casting and hence slurry with high viscosity and finer stucco is preferred. Stucco is applied by dipping the pattern into a

fluidized bed, the rain fall method or simply by hand. The stucco can be silica or aluminosilicate. Each shell coat is allowed to dry for three to four hours depending on the humidity of the surrounding atmosphere. Forced air or fans are sometimes used to expedite the drying process. The shell building process consists of one or two prime coats, four to five back up coats and a seal coat. The backup coats impart strength to the shell and hence coarser stucco is used for this purpose. The coarser stucco also results in more porosity in the shell which can both prevent crack penetration to the surface and increase permeability of the shell. The seal coat uses the same slurry as the backup coats, but uses no stucco. Its purpose is to seal the stucco of the previous layers. The solid investment process [2] is primarily used to produce dental and jewelry castings and has only a small role in engineering applications.

The pattern is then removed from the shell by melting the wax or thermal decomposition of the foam. The shell is cleaned from the pattern residue and strengthened by firing. At the same time, sintering of the ceramic takes place to give the investment casting shell a structure which has enough strength to hold the pressure of liquid metal. If any cracks are found they are repaired by patching with ceramic slurry. Shells are preheated between 700 and 1000°C just before pouring to keep the metal liquid, allowing complete filling of complex geometry parts. During solidification phase transformations take place in the ceramic shell, which results in small changes in volume leading to cracking of the shell. This phenomenon helps in breaking the castings out of the ceramic shells. Once the metal has solidified the shell can be hammered, shot blasted, washed with high pressure water or sometimes chemically dissolved to release the casting. Over the years the process has evolved in order to have better surface finish and

thereby reduce the cost of finishing and machining. Large castings are being poured into free standing shells using this process.

1.2. LITERATURE REVIEW

1.2.1. Thermo-Physical Properties of Ceramic Shells. Hendricks and Engelhardt [4] studied thermal conductivity and heat transfer measurement for ceramic shell molds. In their experiment they plugged one end of an alumina tube with a small amount of wax. Then a ceramic shell of desired composition was built around the end and approximately five cm up the tube. After the shell was completed, including a final drying period, the wax was removed by low temperature firing at around 425°C. A thermocouple was placed on the internal surface of the shell sample. The shell was inserted into a preheated furnace and when the internal temperature reached the target temperature the sample was pulled from the furnace and the cooling profile was recorded. The rate of temperature loss (dT/dt) or the slope of the temperature versus time curve for a number of runs was plotted against temperature. The rate of temperature loss for the test temperature was calculated by linear regression on the slope values within 25°C of test temperature. The authors [4] developed equation for heat transfer through the shell as

$$H = \frac{2(D_S - OD)dT/dt}{3.1416 * ID_2 * (T_i - T_e)}$$

Where H – thermal transfer coefficient, D_s – shell diameter, OD – outside diameter of the tube, dT/dt – rate of temperature loss, T_i – interior temperature, T_e – exterior temperature and ID – inside diameter of tube.

Richards, Lekakh and Druschitz [5] studied dynamic measurements of mold thermal properties with application to the investment casting processes. A novel experimental/computational method was designed for dynamic measurements of the

thermal properties of foundry molds. The method was based on the generation of a precise energy impulse in the mold media by small electrical heater and measurement of the temperature response near the heat source within the molding media. A computer and data acquisition interface was used for controlling impulse cycles and obtaining high resolution temperature measurements. The device had a five mm diameter and could be easily imbedded in different locations within the molds. The coefficient of thermal conductivity was calculated on the basis of the measured temperature response and non steady state heat transfer modeling with fluent software by assuming a constant value of heat capacity. The method has been used for the measurement of the thermal properties of the green sand mold near the surface of the mold cavity during steel pouring and thin ceramic shell properties during de-waxing.

Huang, Berry, Zheng and Piwonka [6] studied the thermal conductivity of investment casting ceramics. These authors [6] mentioned analytical models developed by Eucken and Kingery. Eucken [7] assumed that the pores were spheres and the refractory phase was continuous. The conductivity of the mold, K_m was given by

$$K_m = \frac{K_{S_1} + 2P(1-Q)/(2Q+1)}{1-P(1-Q)/(2Q+1)}$$

Where K_s – thermal conductivity of solid material, K_a – thermal conductivity of air, P – porosity, Q – K_s/K_a.

Kingery [7] assumed the layers would be parallel to the surface (i.e. perpendicular to direction of heat flow). He found that when different ceramic phases were arranged in parallel to the slab plane, the thermal conductivity was given by

$$1/km = [V_1/k_1] + [V_2/k_2]$$

Where V_1, V2 – volume of each phase and k_1, k_2 – conductivity of each phase.

The experimental values of thermal conductivity were measured over the range of 0-750°C using the hot wire method for shells consisting of colloidal silica/fused silica, colloidal silica/zircon, colloidal silica/mullite and colloidal silica/mullite/zircon as well as colloidal silica/alumina and colloidal silica/zircon cores. Simulation theories failed to recognize the heat transfer mechanisms which became more efficient with increasing temperature. For fused silica based shells, values predicted from the model by Eucken and experimental results were observed close to a line, calculated assuming shell is 50% continuous solid and 50% continuous air. Huang et al. concluded existing models could describe the thermal conductivity behavior of monolithic shells up to 750°C if the right percentage of continuous porosity is used in the model. No simple simulation models accurately described the contribution of radiation and translucence to thermal conductivity at high temperatures.

Browne and Sayers [8] also measured the mold thermo-physical properties of ceramic shells. They used an axially located heating element which provided a thermal gradient in a cylindrical specimen of radius 35 mm and length 200 mm. The shell was built up around the element (using the element as pattern) so that good thermal contact would be achieved. Radially located thermocouples were also molded into the specimen and the output was recorded on a data logger. The shell was homogenous i.e. the same slurry and stucco was used throughout. This was done to enable an accurate value of thermal conductivity of the backup part of the shell to be deduced. Thermal conductivity

was determined by applying the Fourier law in cylindrical co-ordinates. The specific heat capacity of the shells was not measured separately but data taken from the thermal conductivity test was used in finite difference calculation to determine the specific heat.

Browne and Sayers [8] continued their work of experimental measurement of investment shell properties. A conventional calorimeter was used to measure the specific heat capacity of a sample of investment material. The sample block was placed in a furnace and brought to the temperature at which data was required. Once thermal equilibrium was established, the test piece was rapidly removed and plunged into the calorimeter. When the new thermal equilibrium was established in the calorimeter, the specific heat of the investment block was measured. Measurements were taken over the range 300 – 1000°C. The data showed a significant increase in the specific heat capacity with increasing temperature.

Connolly, Jones and Marquis [9] measured the specific heat capacity of investment casting shells. The specific heat capacity of the shell was measured using differential scanning calorimeter. Results were compared with calculated values from the rule of mixtures. The rule of mixtures used was

$$Cp_{shell} = f_1C_{p1} + f_2C_{p2} + f_3C_{p3} + \ldots\ldots \text{Etc}$$

Where Cp_{shell} – specific heat capacity of whole investment casting shell, f_1 – fractional mass of material 1, C_{p1} – specific heat capacity of material 1 and so on.

The masses of each coat were measured by drying after each dip and weighed in order to measure the slurry mass loss during heating. Specific heat capacity measurements were taken after each coat. The primary slurry consisted of a 3.7:1 mixture

of zircon and silica as filler in an aqueous based colloidal silica solution with 50/80, 30/80 and 16/30 molochite stucco used for the prime, second and third coat respectively. The specific heat capacity was measured using the differential scanning calorimeter for 1^{st}, $1^{st} + 2^{nd}$ and $1^{st} + 2^{nd} + 3^{rd}$ layers after the samples were fired to 800℃ for one hour. The maximum temperature, for which specific heat capacity was measured, was 750℃. The measured specific heat capacity was then compared with the one obtained using the rule of mixtures. The difference was less than five percent. (Variation of results for differential scanning calorimetry is ± 5%, acceptable). Authors [9] concluded that the specific heat capacity of an investment casting shell can be predicted with a reasonable accuracy using the rule of mixtures.

Sabau and Viswanathan [10] measured the thermo-physical properties of zircon and fused silica based investment casting shells. They [10] treated the investment casting shell as a packed bed. Equations used to measure the thermal conductivity of packed beds were used. The authors [10] measured the thermal conductivity of the prime coat (zircon slurry and zircon stucco) and back up coats (fused silica based slurry and stucco) separately. Shells were prepared with zircon based prime coat or fused silica based backup coats. The hot wire method was used for experimental measurements. The authors [10] observed that the specific heat of the zircon face coat was similar to that of pure zircon and since the zircon face coat did not exhibit radiation effects. The thermal conductivity did not increase with temperature. For fused silica based coats, a third order polynomial fit was assumed to describe the overall shell thermal conductivity since the thermal conductivity of pure fused silica did not vary strongly with temperature. Authors [10] observed that the

thermal conductivity for the ten backup coat shell obeyed the constitutive equation for a packed bed.

Richards, Kruse [11] studied thermal and moisture characterization during autoclave dewaxing in investment casting. Ceramic shells were built on a copper plate. Thermocouples were inserted in the plates, prime coat, back up coats and the seal coat. During autoclave dewaxing, the shell absorbs water and its thermal conductivity drastically changes. By placing a thermocouple on the surface of the shell and the surface of the copper, the temperature of the shell surface and the copper surface were determined. Area of the shell and thickness of the shell being known, thermal conductivity of the shell was determined from the following equation.

$$M_{Cu}.Cp_{Cu}(\Delta T_{Cuc}/t) = (K_sA_s/X_s).(T_{ss} - T_{Cus})$$

Where M_{Cu} = Mass of Copper, Cp_{Cu} = Heat capacity of Copper, t = time, K_s = Thermal conductivity of shell, A_s = Area of the shell, X_s = Avg. thickness of the shell, T_{ss} = Temperature of shell surface, T_{Cus} = Temperature of the Copper surface, T_{Cuc} = Cooper center temperature. It was observed that during autoclave cycle, the thermal conductivity of the shell began at around 0.5 W/mK and as moisture saturated the shell, thermal conductivity of around 1.4 W/mK was achieved.

Many models [12] have been developed to predict the thermal conductivity of two-phase mixtures or porous materials. These models include the series model, parallel model, Eucken model, Kingery model, Russell model, Son Frey model, Rayleigh-Devries model, Maxwell model and the Bruggeman model. The equations of these models are summarized in appendix table 3. These models can be applied to a ceramic shell by

taking into account the thermal conductivities each phase, the continuous phase (solid ceramic) and the discontinuous phase (porosity), and the volume fraction of each.

Attempts were made to use these models to predict the thermal conductivity of investment casting shells. It was observed that the models don't accurately predict the thermal conductivities of the ceramic shells. First, the ceramic shell is not a continuous phase but a mixture of two or more phases like fused silica, zircon, aluminosilicate etc. Each of these materials conducts heat differently. Hence the term K_c in the models should be modified to a new term taking into account the thermal conductivities of all solid phases. Second, the thermal conductivity models fail to account for the effect of connected porosity. Connected pores will have a significant effect on the term used in the models (K_d). Third, the process parameters (binders, viscosities of the slurry, stucco application method, pattern removal methods, firing processes etc) used during the shell building process can have considerable effect on properties such as the pore sizes and the layered structure of ceramic shell. The models fail to consider any of these parameters.

It was observed that the thermal conductivities and specific heat capacities measured varied for the research done so far. They are summarized in appendix table 1 and table 2. There is no substantial data which is accepted by commercial simulation software. This study was intended to contribute to the database for modeling investment casting.

1.2.2. Metal – Ceramic Shell Interactions. With technological advances like rapid prototyping, CNC foam machining, the investment casting industry is moving towards large and geometrically complex parts. Although it is possible to cast these parts

successfully using the investment casting process, there are certain areas which need more attention. With an increase in size there has also been an increase in solidification time of the castings. Complex geometry led to variations in the temperature history different regions of the solidifying casting. As a result the ceramic shell can experience high temperature in certain regions for considerable time which could lead to metal-ceramic shell interactions.

Metal-mold interactions have been studied for decades in the casting industry but most of the work was dedicated to the study the specific burn-in/burn-on surface defect formation when using green sand and wash-coated no-bake sand molds.

Gililland [13] conducted experiments by casting grey, ductile iron and steel into sand molds and examined the effect of hot metal on sand adherence with a scanning electron microscope. Special attention was given to the effect of hot spots on sand burn-in. Molds were extensively instrumented with thermocouples to obtain time-temperature data in locations like hot spot interfaces, cold spot interfaces, and different locations in the sand away from casting. Gililland [13] observed that the interface temperature reached the solidus. Examinations of the metal and sand surfaces had been performed using energy dispersive microprobe analyzer. Microprobe analysis of the reaction interface showed that Fe, Mn, Si, P and Ni were the major components.

Brooks, Beckermann and Richards [14] developed a method to predict burn on and penetration defect locations using casting simulation. The suggested method for burn-on prediction is based on the simulation of the locations where mold is above a certain

critical temperature, generally above the steel solidus temperature, while adjacent casting regions have not yet solidified.

Richards [15] studied mold-metal penetration in steel castings. Zircon coatings are used for cores and in the molds because of various advantages of like greater surface tension at the mold metal interface, lower thermal expansion etc. The higher thermal conductivity of the zircon coating leads to more rapid solidification of the casting surface skin. In the first case study, extensive penetration in a zircon core located beneath the riser was analyzed. Metallographic and SEM analysis revealed that the integrity of the coating was an important issue. Failure of the coating was due to flaws produced during drying, shrinkage giving rise to stresses, failures due to variation in coating thicknesses which lead to mechanical pressure driven penetration. Another possibility observed was localized decomposition of zircon to zirconia and silicate glass. This phenomenon could be important due to the sixteen percent difference between in the thermal expansion of zirconia and zircon.

Two more case studies [16] were performed for a zircon sand core in a lightener pocket of a thirty-two ton large gear casting and a thin piece of adherent sand from zircon wash coated green sand mold using chromite and zircon sand mixed. Polished section examination of a penetrated core sample revealed pressure driven flow rather than capillary action. SEM also revealed a reaction product containing aluminum, silicon, iron and manganese oxide. Zircon showed a tendency to form a liquid reaction product and zirconium oxide, in equilibrium with the reoxidation products such as FeO and MnO. This suggested that coatings will perform better when foundry practices limit reoxidation product formation. Zircon coatings will not survive extended contact with a liquid phase

formed from reoxidation products. The following conclusions [17] were drawn from fundamental understanding of the mold penetration phenomenon and various case studies: (1) Coating failure could be due to exceeding the coating toughness limitations during drying, core material thermal expansion or thermal shock, (2) material handling effects can damage the coating and (3) localized decomposition of coatings, for example, zircon to zirconia and silicate glass, when in contact with a liquid reoxidation product.

Rasquinha, Richards [18] studied burn in/burn on case studies on samples from different commercial foundries. Analysis showed one of the causes for burn in/burn on was liquid chemical reaction penetration mechanism. Thermodynamic analysis of the reaction product showed it was substantially liquid at steel pouring temperatures. Steel can become partially oxidized during pouring and the reaction product can possibly form by the reaction between partially oxidized steel and the mold coating zircon. It was observed that unlike steel which does not wet silica sand, iron oxide readily wets and dissolves silica sand. In addition to the formation of liquid oxide at mold metal interface wetting the sand and allowing burn in and burn on, liquid phase sintering also occurs causing the sand near the surface to densify non-uniformly, thus leading to disruption.

Richards, Kruse [19] studied burn in/ burn on with respect to coating characterization. Parameters assessed were composition, density, viscosity of the coat, surface geometry, drain angle of cores and molds. As solids' loading was decreased for a coating the degree of penetration increased and the layer thickness on the surface of sand decreased. At optimal solids loading there was less effect of the drain angle on coating quality. The pseudoplastic nature of the coatings suggested yield stress for flow was an important indicator of ability to resist runs and thick spots in coating.

Hayes, Barlow, Stefanescu, Piwonka, Owens, Lane [20,22,23,24] studied mechanical penetration of liquid steel in sand molds. Sessile drop experiments were run to evaluate the effect of steel chemistry on contact angle for different substrates. The sessile drop data was used to develop a mechanical penetration model. The model was based on the following equation.

$$P_{st} + P_{dyn} = P_y + P_{gas} + P_f$$

The static pressure (P_{st}) and dynamic pressure (P_{dyn}) promote penetration, whereas capillary pressure (P_y), gas pressure (P_{gas}) and frictional pressure (P_f) oppose it. A penetration index was defined as the ratio of actual contact angle between the molten steel and mold aggregate and the critical contact angle was calculated. The model gave satisfactory results for different metallostatic heads, carbon contents etc. It was observed that the mechanical penetration can occur in all ferrous castings. When mechanical penetration occurred, no reaction between the sand and the steel was observed. The variables that influence its occurrence the most were metallostatic head, metal velocity in the mold and grain size of the molding aggregate. Steps suggested to eliminate mechanical penetration were the application of the mold coating, decreasing the flow rate of the metal into the mold and choosing a molding aggregate that is less susceptible to wetting.

Hayes, Barlow, Stefanescu, Piwonka, Owens, Lane [21,22,23,24] also studied chemical penetration in sand molds in steel castings. A thermodynamic model for the evaluation of critical carbon content (minimum carbon content required at interface to prevent iron oxidation) was created. Steel castings were poured in different mold materials like green

sand, sodium silicate, furan sand etc. Probes for the sampling of gases were placed in molds with and without cores. Gases were analyzed with a mass spectrometer and gas chromatograph. Cross sections of the castings were viewed optically as well as with a scanning electron microscope to determine the extent and type of penetration present. Also experiments were performed to study the evolution of the contact angle of steels of different chemistries on a variety of substrates like silica, alumina, mullite, olivine, zircon, chromite etc.

It was observed that the more oxidizing the mold atmosphere caused chemical penetration. High carbon steels were less prone to penetration defects than low carbon steels because the high carbon protects the metal from oxidizing. The atmosphere at the mold-metal interface during solidification of steel depended on the type of binder, specifically mold carbon and moisture content. All uncoated sand molds regardless of binder composition suffered chemical penetration, indicated by iron oxide and fayalite found on casting surface. It was observed that iron oxide produced a FeO layer next to the steel matrix and a fayalite layer next to silica sand. Sessile drop experiments revealed that most ceramics, with the exception of olivine and chromite were suitable for carbon steels in neutral atmosphere. For stainless steels the best performance was observed for zircon, alumina and magnesite molding materials. High Mn steels were found to be compatible only with alumina and magnesite based sands. Silica sand should be avoided since it forms low melting eutectic with MnO resulting from the oxidation of Mn in the steel.

Colligan, Van Vlack, and Flinn [25] studied factors affecting metal-mold interactions by casting AISI 1080 steel in green sand molds and resin bonded sand molds

with different *Mn* contents. The effect of Mn additions and atmosphere on interface reaction was qualitatively evaluated. The authors [25] explained the interaction phenomenon on the basis of penetration and interface reaction, Mn addition and mold material effect. The surface finish and interface reaction zone exhibited a pronounced influence of Mn by extensive liquid silicate melt formation over entire range of Mn additions. The atmosphere produced by phenolic resin bonded shell molds, oxidized to a lesser degree than that of green sand molds, resulted in slight interface reaction over the range of Mn content.

Tani, Ueda, Mori [26] studied interfacial reaction between cast steel and olivine sand. Authors [26] observed that Mn in molten high Mn steel volatilized and penetrated mostly through serpentine and cracks in the olivine sand grains. The penetrated Mn lowered the melting point on the surface of the olivine sand grains and a partially fused layer was formed at the metal-mold interface. A similar reaction was observed in green sand. Comparison was made between the olivine sand and silica sand, and the effect of Mn coating on the olivine sand grains against burning was investigated in their work.

Cingi, Vainola, Orkas [27] studied the role of oxygen in mold-metal interactions in investment casting of magnesium alloy AZ91E. They [27] observed during pouring and filling that the Mg melt reacted with oxygen and the formed MgO reacted with the mold material. External oxygen reacted with Mg melt after filling and caused mold-metal reactions. Thermodynamic calculations indicated the function of free oxygen is to react with Mg melt and supply energy for the mold-metal reaction to occur. The authors [27] recommended that the shell should be flushed with protective gas such as SF_6 to eliminate reactions. Authors [26] also suggested that in order to eliminate reactions due to

external oxygen, shell molds should be sealed by either a glaze layer or by applying an additional layer of zircon on the sintered mold.

Jones, Marquis and Page [28] characterized thermal profiles and metal-mold interaction within investment casting molds. Two types of molds (5kg and 60 kg) were prepared with a prime coat consisting of zircon based slurry and zircon stucco, back up coats were made with the same slurry and molochite stucco. Thermocouples were inserted into the pattern and at different levels in the shell to measure the temperatures at each coat of the shell. Shells were poured with martensitic stainless steel and low alloy steel. For the 5kg mold authors observed some alloying elements appeared to have leached or diffused into the mold structure, possibly through melting of the binder followed by capillary action. The interactions appeared to be 85 μm deep inside the shell after which the structure was unaffected by metal. For 60 kg mold aluminum, zirconium, iron, sodium etc were observed, possibly due to partial melting, to a depth of approximately 75 μm. The authors [28] observed more interaction layer in the 60 kg mold due to the fact that primary coats of the mold were at high temperature for longer periods of time which allowed the refractories to melt and recrystallize during cooling.

Zhang, Morin [29] studied the effect of inhibitor gas on mold-magnesium reactions in investment casting. Ceramic shell molds with different binder and refractory particles were prepared for pouring AZ91 magnesium alloy. Inhibitor gas was guided into the shell molds for removal of oxygen and formation of barrier between the mold and the magnesium. The results of experiments showed that a mixture of CO_2 and proper concentration of SF_6 used as inhibitor gas can effectively limit mold-magnesium reactions. A surface analysis with auger electron spectroscopy and electron spectroscopy

for chemical analysis had been performed on the surface of magnesium parts cast under inhibitor gas. It was discovered a special layer appeared on the part surface, in which elements such as magnesium, oxygen, fluorine, aluminum, sulphur, silicon etc were detected.

Sikkenga [30] analyzed gases in air melt investment casting alloys. He [30] suggested it was easier and more effective to limit gas pickup than it was to attempt any substantial removal of gas in the foundry. He recommended following ways to minimize negative effects of gases in cast metals.

1. Start with lowest oxygen melts stock available.
2. Keep superheats low.
3. Keep melting times as short as possible.
4. Use an effective argon cover to prevent gas absorption.
5. Minimize additions to melt.
6. Use only dry refractories.
7. Realize the potential for entrapped air which exist with primary vertical gating arrangements.
8. Adequate pouring practice to prevent reoxidation.

1.3. FOCUS OF RESEARCH

Most of the work done so far in the thermo-physical properties measurement of ceramic shells was limited to the maximum temperature of 800°C. It was also observed that the thermal conductivity models developed cannot be directly applied to predict the thermal conductivity of the ceramic shell. The porosity in the shell structure accounts for the considerable variation in the measurement of thermo-physical properties. Hence it is necessary to measure the thermo-physical properties at the temperatures higher than 800°C, close to the steel castings temperature as possible.

This research deals with thermal conductivity and specific heat capacity measurements at temperature up to 1200°C of different compositions of investment casting shells. The obtained data will be incorporated in Magmasoft and will be used for simulation of the investment casting process.

Metal-mold interactions have been studied by many authors but most of the work was done on wash coated sand molds and burn in/on. Hardly any work has been done for steel-ceramic shell interactions in investment casting. With growth of the steel investment casting industry, increasingly complex geometry and larger sizes of the castings, this phenomenon has received more attention. Also due to the complex structure of the ceramic shells and the limited scope of thermal measurement techniques, thermodynamic modeling is not easy.

During an industrial trial for a casting of complex geometry which was conducted by Missouri S&T, the presence of interaction products was observed and hence this study was undertaken. This work combined Magmasoft simulation and Factsage modeling to

study metal-mold interactions. The comparison of thermodynamic predictions and experimental results helped to provide recommendations for material selection for shell making. It can also contribute to understand the foundry practices to limit the reaction.

2. EXPERIMENTAL PROCEDURES

2.1. SLURRY PREPARATION

The slurry used for making investment casting shells plays a major role in determining final properties of the mold such as thickness of the shell, permeability, strength etc. The flours used were fused silica, zircon and alumina. The binder used, Megasol contained 45 wt% amorphous silica (in suspension) and less than one weight percent sodium hydroxide in water solution. The flours used were Ranco-Sil fused silica, alumina and zircon. The flour and binder were combined in a 2:1 weight ratio. Initial, high shear mixing of the ingredients was done using 333 RPM/40 HP, DC motor. Once the flour was adequately dispersed into the binder, the bucket containing the binder and the flour was placed onto a plate rotating at 15.7 RPM with a scraper bar, as shown in figure 2.1. The scraper bar helped to prevent the solids from settling.

Figure 2.1 Mixing plate and scraper bar shown with an empty mixing bucket

After preparation, the slurry was left under low shear for minimum of twelve hours to allow air bubbles which were introduced during flour addition to float out. Once the entrapped air had escaped the slurry and the slurry's viscosity had stabilized, the viscosity of the slurry was tested using a Brookfield DV-II + Pro viscometer with a LV3 spindle operating at 30 RPM as shown in Figure 2.2. The LV3 spindle was selected because the viscosities tested were well within its testing range. Based on previous trials at Missouri S&T a spindle speed of 30 RPM was selected.

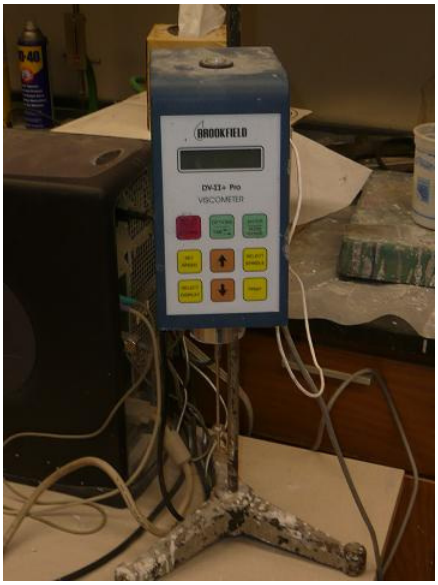

Figure 2.2 Brookfield DV-II+ Pro viscometer used to measure slurry viscosity

To lower the viscosity of the slurry, de-ionized water was added in controlled volumes. The added water was given minimum of fifteen minutes to disperse throughout the slurry before additional rheological readings were taken. In the event that viscosity of

the slurry was below the target range (700-1000 cP), natural evaporation was used to lower the water concentration.

2.2. PATTERNMAKING

The surface of the pattern is another important parameter since it's replicated to the interior surface of the ceramic shell which in turn is responsible for surface quality of the castings. High density (EPS) foam was used to make the patterns for both thermo-physical property measurements as well as steel-ceramic shell interactions study. In order to obtain the final shape of the designed pattern pieces cut from the foam were glued together and the final required design was constructed. To promote the slurry wetting on the pattern, the surface of the foam was modified using 150-grit sandpaper.

2.3. PATTERN COATING

When the viscosity of the slurry was in the target range, the pattern was dipped for coating. Either the top inch or the attached pouring cup of the pattern was used as grip area while the rest of the pattern was submerged into the slurry for at least five seconds and then rotated 360° to allow all parts to be fully coated. The pattern was then gradually removed from the slurry to allow excess slurry to naturally drain off. The patterns were held at 45° angle to the horizontal and were rotated along their axis. The rotation prevented over draining from a single edge thus created a uniform coating thickness across the surface. Once the interval between the drips from the shell exceeded three seconds, stucco was applied using the rainfall method where the stucco was sprinkled onto the pattern through a grated container suspended two feet above the pattern. The

pattern was rotated so that dipped surface gets coated uniformly and no area was missed. The stuccos used were Ranco-Sil fused silica, aluminosilicate and zircon.

2.4. SHELL FIRING

The prepared shells were fired at 900°C with heating rate of 3°C/min, were held at 900°C for four hours and then furnace cooled to the room temperature. After firing all shells were checked for any visible cracks. Shells obtained from industrial foundries used the same pattern designed at Missouri S&T and were fired with the same parameters.

2.5. DENSITY MEASUREMENT BY ARCHIMEDES METHOD

An experimental procedure [3,38] based on ASTM C20 was used for density measurement of investment casting shell samples. Samples of approximately 1”x 1” x 0.4” were cut from the fired shells were then heated to 150°C for minimum of one hour and then allowed to cool to the room temperature. The samples were weighed immediately to determine their dry weight (without moisture). Then the samples were placed in an aluminum wire cradle. The cradle was suspended from wire supports on top of one liter beaker filled with water. The samples were allowed to hang freely in water without coming in contact with other samples or beaker floor or walls. Once the samples were placed, the beaker was placed on hot plate for boiling. Following two hours of boiling, the heat source was turned off and the water was allowed to cool back to room temperature overnight. Without removing the samples from the water, the wire cradles holding the samples were moved to a hanging weight scale one at a time. The differences between submerged cradles’ weight with and without shell samples were recorded. When removing the samples, care was taken not to draw out water from within the sample. For

this, contact with hands was minimized to only small patches on sides and the samples were suspended by plastic clamps. The samples were weighed a third time by suspending them in air while still wet. The apparent porosity and bulk density of the samples were calculated from the following equations taken from ASTM C20.

$$P_{app} = \frac{W_W - W_D}{W_W - W_S} \times 100\%$$

$$B = \frac{W_D}{W_W - W_S}$$

Where W_D is dry sample weight, W_S is the submerged sample weight and W_W is wet sample weight. (All measured in grams)

3. THERMO-PHYSICAL PROPERTIES OF CERAMIC SHELLS

Ceramic shell molds have complex structure and phase transformations that occur during both firing and pouring thermal cycles. These factors influence the thermal properties of the shell mold. Knowledge about the time and temperature dependency of heat capacity and heat conductivity is important for investment casting process development and computational simulation of casting solidification.

Thermo-physical properties of investment casting shells include specific heat capacity, thermal conductivity, gas permeability, density and surface emissivity. All of them play an important role during casting solidification. This research is focused on measuring the *Cp* and *K* of investment casting shells.

When investment casting shells are poured, heat is transferred through three different heat transfer mechanisms, conduction, convection and radiation. It is difficult to measure the thermo-physical properties for many reasons. First, the shell is composed of layers with different thermal properties. Second, each layer is composed of binder and refractory which conduct heat at different rates. Third, the porous structure presents computational difficulties because some pores are connected to pores in adjacent layers. Fourth, there is a glassy phase is formed in the shell at elevated temperatures which conducts heat locally by radiation.

The measurement techniques used in this study are differential scanning calorimetry and laser flash thermal diffusivity. Also it was important to compare experimental data on heat capacity of pure components with multi-layered shells in the green condition, during firing and pouring cycles. The purpose of this study was to

understand whether process temperature history has a significant effect on shell thermal properties.

Shells prepared around wax or foam patterns during investment casting are subjected to high temperature cycles from pattern removal, firing, preheating just before pouring and finally during casting pouring and solidification. High temperature thermo-physical properties including thermal conductivity (*K*) and specific heat capacity (*Cp*) of the shell materials influence all these processes. Powerful simulation software like Magmasoft for metal casting processes have been developed and are commercially available. Properties of the known and newly developed alloys as well as those of the mold materials used need to be included in the software databases. The reliability of the model depends on including accurate materials properties in the database. In application, it must be considered that these thermal-physical properties depend significantly on temperature and process history.

3.1. SHELL PREPARATION

Three different types of shells were prepared in the Missouri S&T foundry to determine the effect of the refractory materials used on the specific heat capacity and thermal conductivity of investment casting shells. Two industrial foundry shells (foundry A and foundry B) were also tested for comparison. Foundry A had zircon based prime coat and aluminosilcate as stucco in back up coats. Foundry B had fused silica based prime coat and coraser mesh silica as stucco in the back up coats. Table 3.1 shows the materials used for shell preparation. Shells prepared in the Missouri S&T foundry had one prime coat, five back up coats and a seal coat. All the shells were fired to 900°C for

three hours before testing. The percentage of open porosity in each type measured by Archimedes method is shown in appendix table 4.

Table 3.1 Compositions of shells prepared at Missouri S&T lab for Cp and K measurement

Type of shell	**Binder**	**Flour**	**Stucco**	**% Open porosity**
Fused silica	Colloidal silica	Fused silica	Silica 30-50 mesh	13.64
Fused silica + Zircon	Colloidal silica	Fused silica + fused zircon	Silica 30-50 mesh	9.38
Fused silica + Aluminosilicate	Colloidal silica	Fused Silica	Aluminosilicate 30-60 mesh	14.48
Foundry A	Colloidal silica	Zircon	Aluminosilicate	21.57
Foundry B	Colloidal silica	Fused silica	silica	17.86

3.2. LASER FLASH TEST

The laser flash test [31] is used to determine the thermal diffusivity of primarily homogenous isotropic solid materials. Thermal diffusivity values ranging from 10^{-7} to 10^{-3} m^2/s are readily measurable by this test method from about 75K to 2800K. This method is typically applicable to fully dense materials; however, in some cases it has shown to produce acceptable results when used with porous samples. The magnitude

of porosity, pore shapes, sizes and parameters of pore distribution influence the behavior of thermal diffusivity.

The essential components of the apparatus are a flash source, a specimen holder, an environmental enclosure, a temperature response detector and a recording device. The flash source generates a short duration of pulse, less than 2% of the time required for the rear face temperature rise to reach one half of its maximum value to keep the error due to finite pulse width less than 0.5%. An environmentally controlled chamber is required for measurements above and below room temperature. The detector provides a linear electrical output proportional to a small temperature rise. The data acquisition system is of adequate speed to ensure that time resolution in determining half of the maximum temperature rise on the thermogram is at most one percent for the fastest thermogram for which the system is qualified.

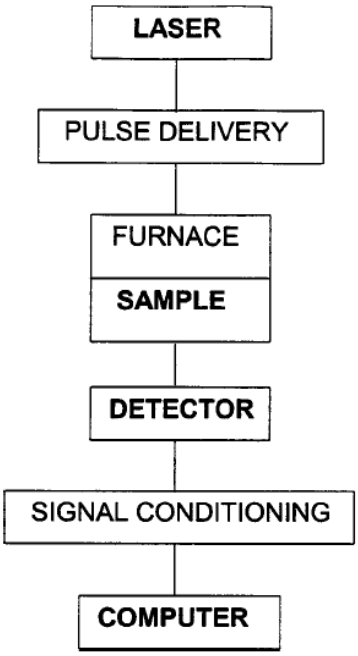

Figure 3.1 Block diagram of a laser flash system

In the laser flash test [31,32] a small thin disc of the specimen is subjected to a high intensity short duration radiant pulse. The energy of the pulse is absorbed on the front surface of the specimen and the resulting rear face temperature rise is recorded. The thermal diffusivity value is calculated from the specimen thickness and the time required for the rear face temperature to reach certain percentages of its minimum value.

Assuming ideal conditions, the temperature response on the rear face of the specimen is obtained by the one dimensional equation:

$$\Delta T = \Delta T_m \left[1 + 2\sum_{n=1}^{\infty} (-1)^n \exp\left(\frac{-n^2 \pi^2 \alpha t}{L^2} \right) \right]$$

where: α is the thermal diffusivity, L is the thickness of the specimen, ΔT is temperature rise of specimen, ΔT_m is maximum temperature rise of the specimen and t is the time after pulse heating. When the temperature reaches $\Delta T/\Delta T_m$ time is set as $t_{1/2}$ and the thermal diffusivity (a) can be calculated from the following equation:

$$\alpha = \frac{0.1388 L^2}{t_{1/2}}$$

In the laser flash test, a reference specimen (graphite) and the test specimens (shells), are mounted together under the same conditions and irradiated uniformly with a laser beam. To insure similar emissivity, the front and rear faces of both the reference and the test specimens were covered with a graphite spray coating. Thermal diffusivity values are measured from transient temperature curves on the rear face of both specimens by a curve fitting method. The rear face temperature rise of the reference (graphite) with known specific heat capacity and the specimen are measured with non-contact infrared radiation thermometer. If the density (ρ) of the specimen (shell) is known then specific heat capacity (c_p) of the shell can be calculated from following equation:

$$\left(\rho c_p\right)_M = \frac{L_R \Delta T_R}{L_M \Delta T_M}\left(\rho c_p\right)_R$$

Where: L_R and L_M are the thicknesses of the reference and specimens, respectively.

Thermal conductivity (K) of the shell can be calculated by substituting measured value of specific heat capacity into following equation

$$K = \rho Cp \alpha$$

Following figure 3.2 shows the laser flash equipment (FLASHLINE™ 5000, Anter Corporation) used for the study.

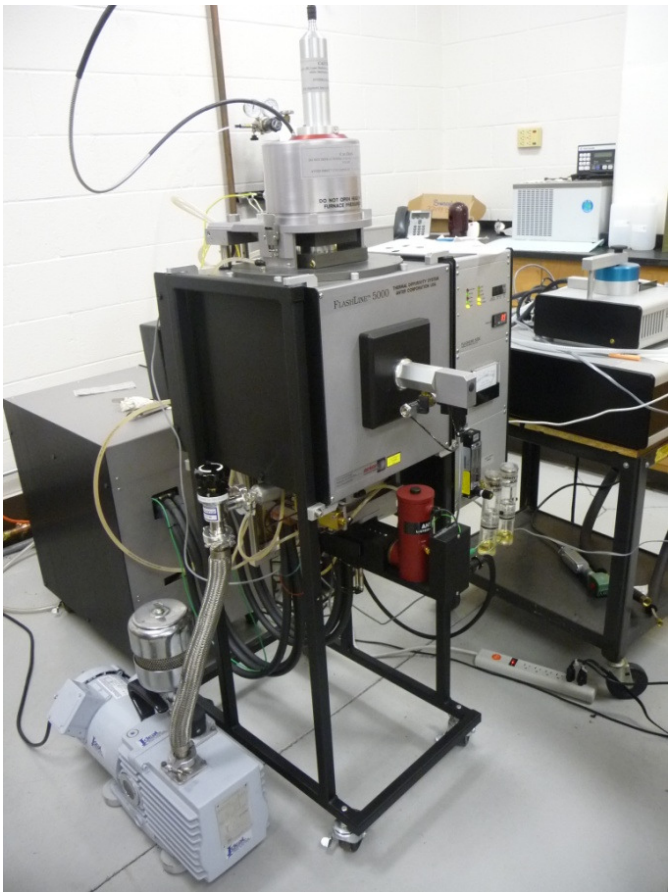

Figure 3.2 FLASHLINE™ 5000 (Anter Corporation) laser flash equipment

To prepare laser flash test samples, small samples were cut from the fired shells. The final sample size of 12.7 × 12.7 mm and two mm thick was achieved by grinding to ensure they have exactly flat surfaces. The laser was flashed on the prime coat side of the shell. Figure 3.3 shows the samples before and after graphite coating.

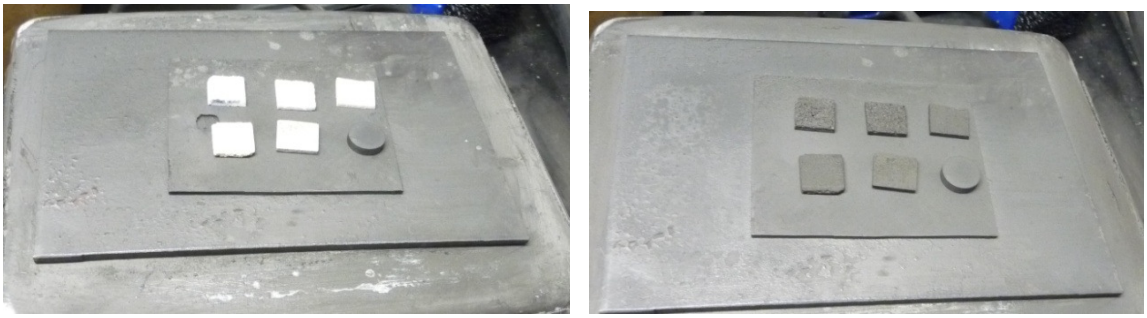

(a) (b)

Figure 3.3 Samples and standard (a) before graphite coating and (b) after graphite coating.

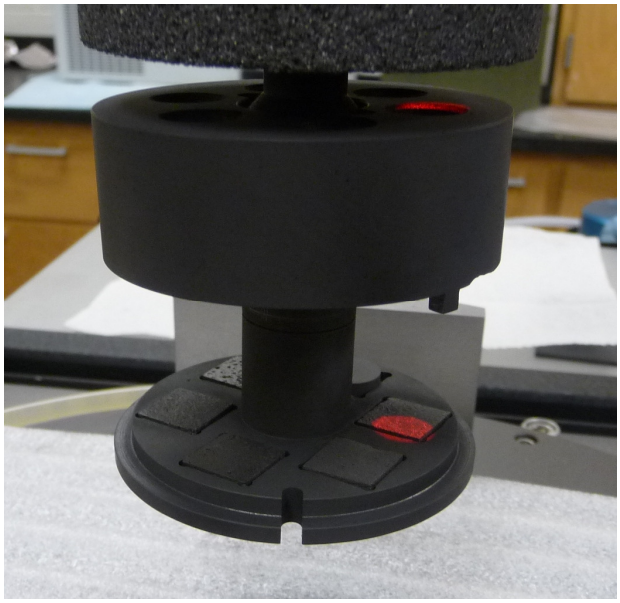

Figure 3.4 Shell samples and standard placed in holder before laser flash test

For measurement of thermal diffusivity, required temperature was stabilized, three laser shots were taken and average of the three was recorded. The laser flash operating program requires sample thickness to be entered before it starts a run. Thermal diffusivity values were obtained from 200°C to 1200°C at the intervals of 100°C. The laser flash equipment runs a built in standard to measure thermal diffusivity. Densities of the samples were measured using Archimedes method. Four runs of each type of sample were conducted in laser flash test and the average values are reported in results.

3.3. DIFFERENTIAL SCANNING CALORIMETRY (DSC)

Differential scanning calorimetry (DSC) determines the temperature and heat flow associated with material transitions as a function of time and temperature. It also provides quantitative and qualitative data on both endothermic and exothermic reactions occurring in materials during phase changes, melting, oxidation, and other heat related changes.

In DSC, a sample and an inert reference are heated at a known rate in a controlled environment. The increase in the temperature of the sample and reference will be the same unless an endothermic or exothermic reaction takes place in the sample. The temperature difference between sample and reference during such a heat change is directly related to the differential heat flow.

The sample and reference thermocouple are connected in series opposition (back-to-back) so that if the sample and reference temperatures are same, the resulting electrical potential is zero. If the sample temperature is higher than the reference, the output electrical potential is one polarity; if the sample temperature is lower, the polarity is

reversed. DSC measures the differential voltage between the thermocouples at the sample and reference platforms.

Phase transformations in silica play an important role during firing, preheating and pouring in the investment casting process. Hence it is necessary to understand the effect of process history on the specific heat capacity of the shell. Fused silica based shells were tested using DSC to study the effect of phase transformations on specific heat capacity of the shell. Three different types of samples were measured: green or unfired shell, shell fired to 800°C and shell fired to 1200°C. Each type of sample was heated at the rate of 15°C/min to 1200°C and then held 1200°C for one hour before cooling down to room temperature. Samples were then given another run with the same 15°C/min heating rate to 1200°C and cooled down to room temperature.

3.4. RESULTS

Figure 3.5 shows an example of raw data obtained from laser flash method.

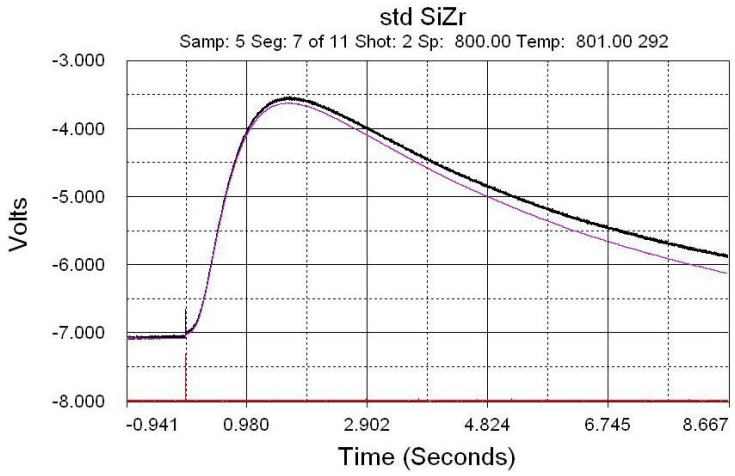

Figure 3.5 Example of thermal diffusivity measurement of reference and sample

Figure 3.6 to Figure 3.10 show the C_p results obtained for Missouri S&T and industrial shells with using laser flash method. The specific heat capacity substantially increased with increasing temperature in all cases.

Figures 3.11 to 3.13 show the results of DSC of fused silica based shells. Three different types of samples were measured: green shell, shell fired to 800℃ and shell fired to 1200℃. Each type was heated at the rate of 15℃/min to 1200℃ and then held at 1200℃ for one hour before cooling to room temperate. Samples were then run again with the same procedure.

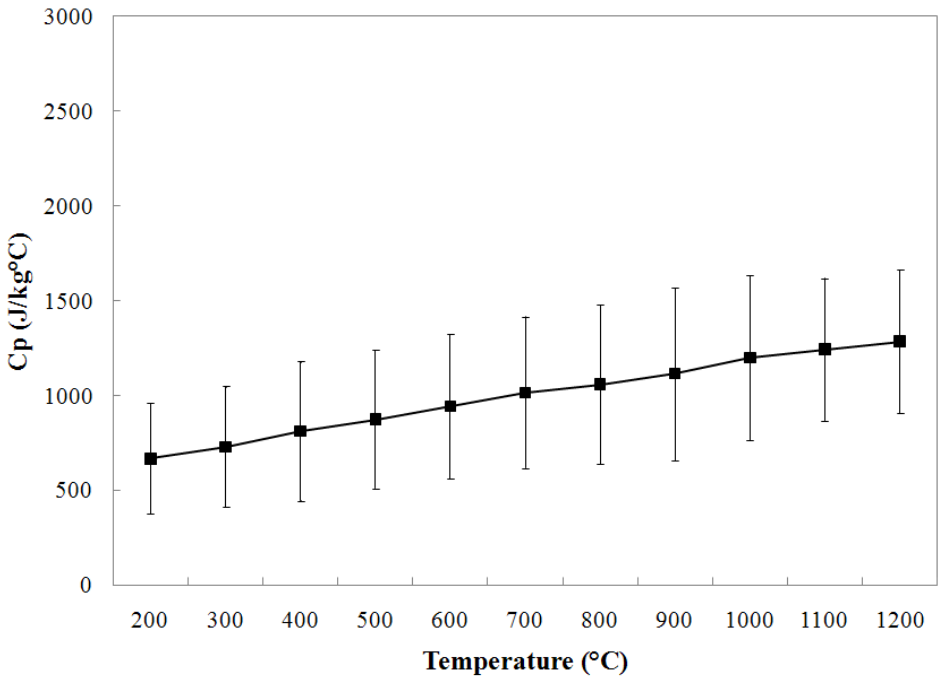

Figure 3.6 Specific heat capacity of the silica shell prepared at Missouri S&T foundry from the laser flash test (fired at 900°C)

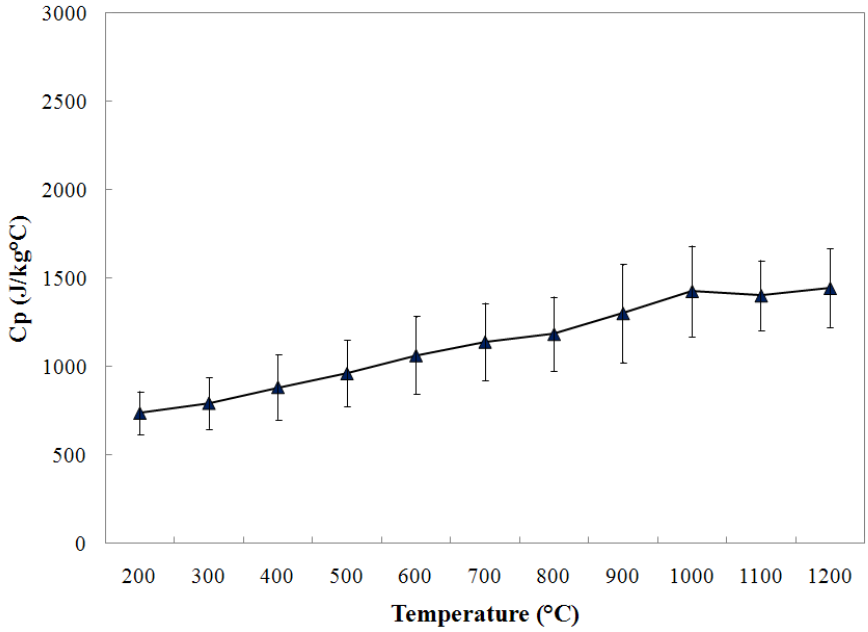

Figure 3.7 Specific heat capacity of the silica + zircon shell prepared at Missouri S&T foundry from the laser flash test (fired at 900°C)

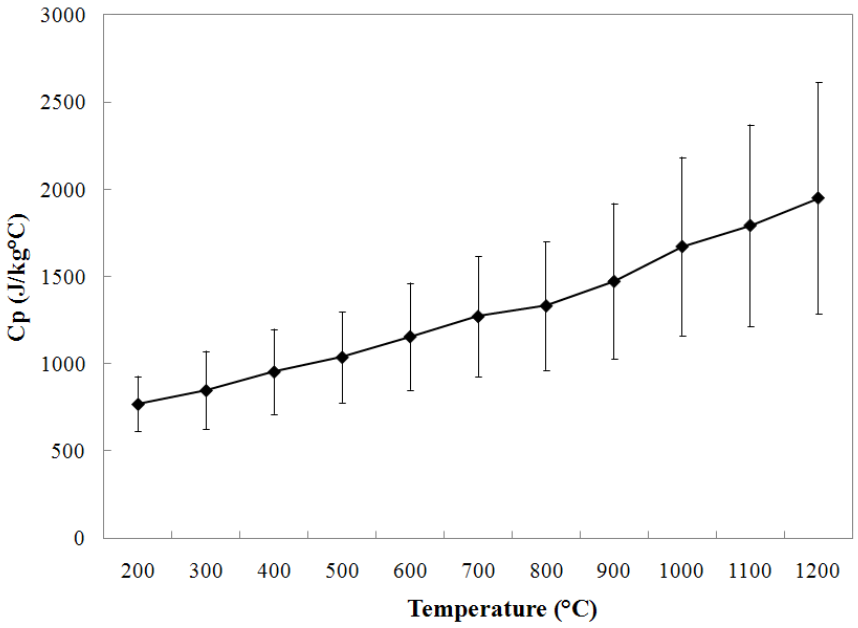

Figure 3.8 Specific heat capacity of the silica + aluminosilicate shell prepared at Missouri S&T foundry from the laser flash test (fired at 900°C)

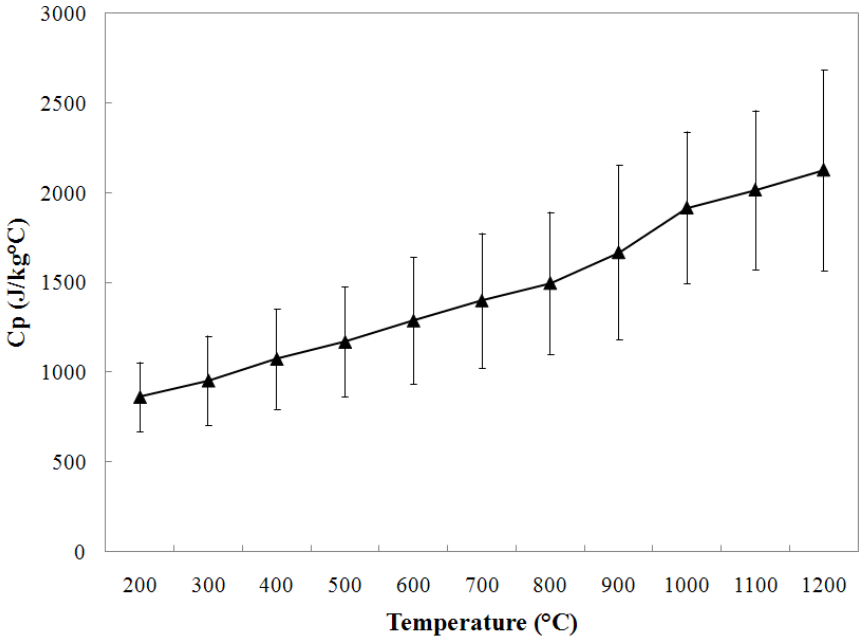

Figure 3.9 Specific heat capacity of the shell (fired at 900°C)

measured by the laser flash test for foundry A (flour – zircon, stucco – aluminosilicate)

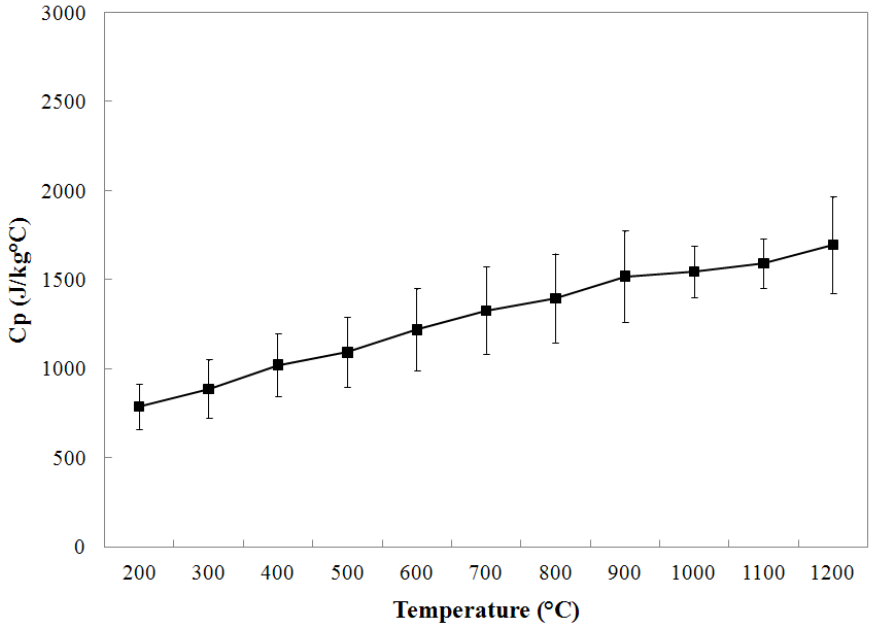

Figure 3.10 Specific heat capacity of the shell (fired at 900°C)

measured by the laser flash test for foundry B (completely fused silica based)

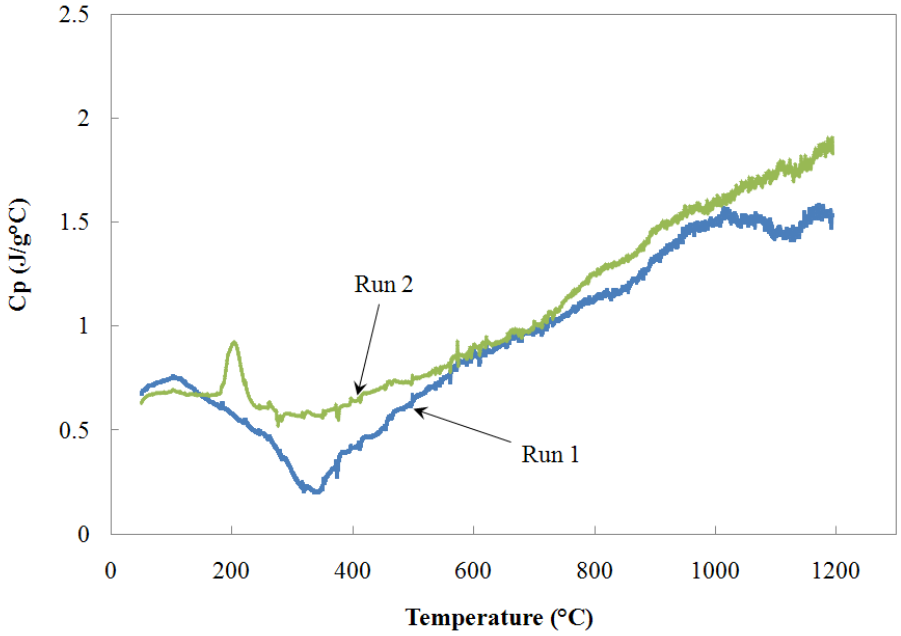

Figure 3.11 Specific heat capacity of fused silica based shell not fired (Run 1-first firing heating of green shell and Run 2 - second heating cycle the same shell)

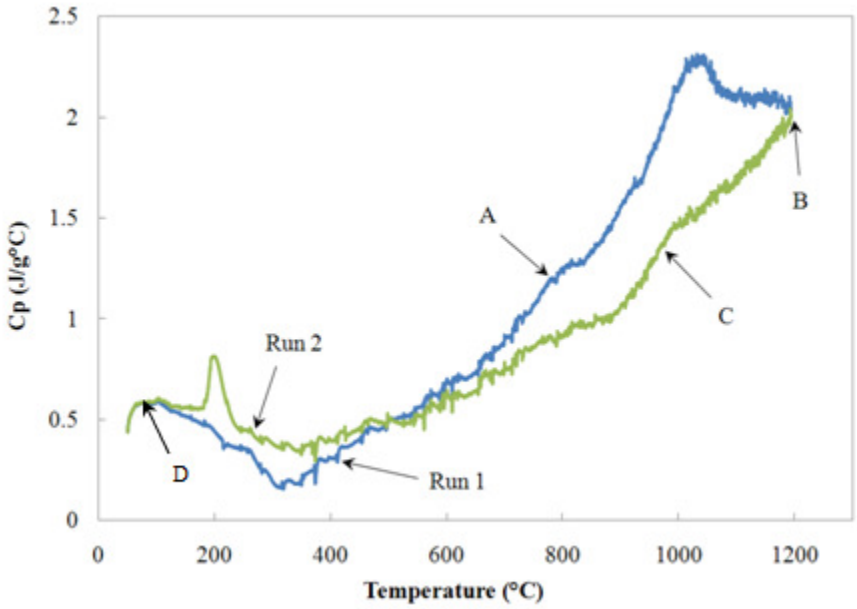

Figure 3.12 Specific heat capacity of fused silica based shell fired to 800°C (Run 1-first firing, heating of green shell and Run 2 - second heating cycle the same shell)

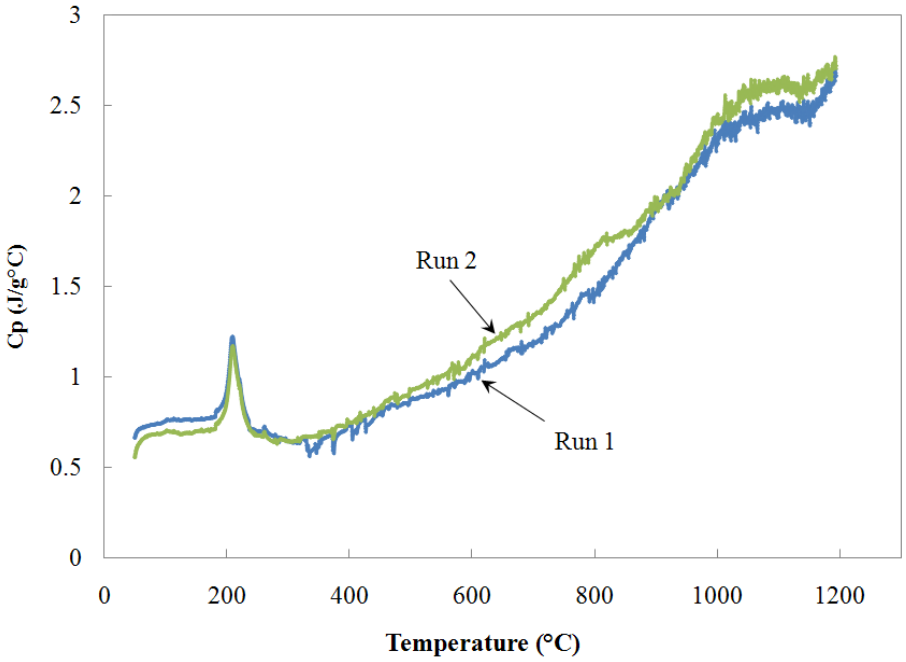

Figure 3.13 Specific heat capacity of fused silica based shell fired to 1200°C

(Run1 - heating cycle of preliminary fired at 800°C shell and

Run 2 – second heating cycle the same shell)

Figure 3.14 to Figure 3.18 show thermal conductivity measurement results for Missouri S&T and industrial shells. Thermal conductivity increased for all type of shells with the increase in the temperature.

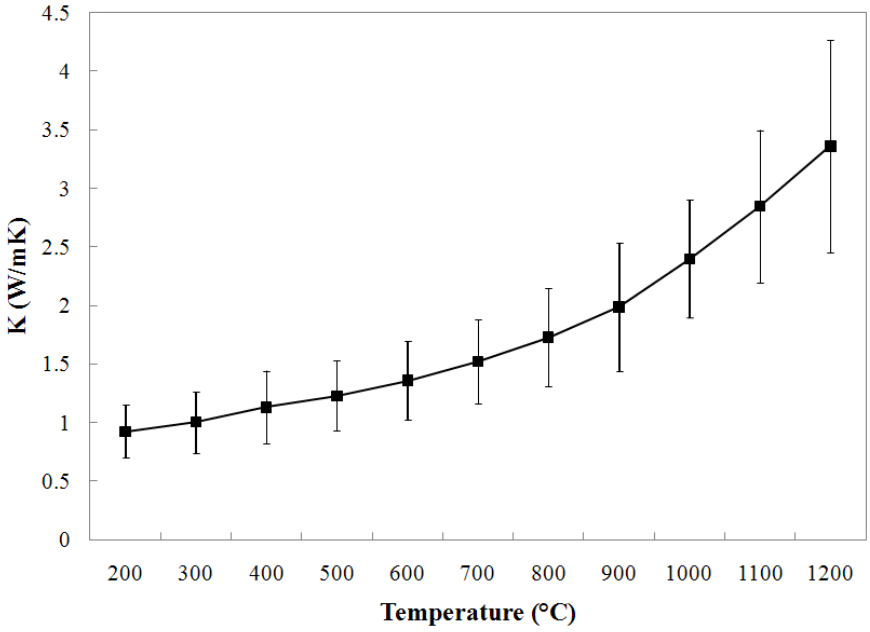

Figure 3.14 Thermal conductivity of the silica shell prepared at Missouri S&T foundry (fired at 900°C) by the laser flash test

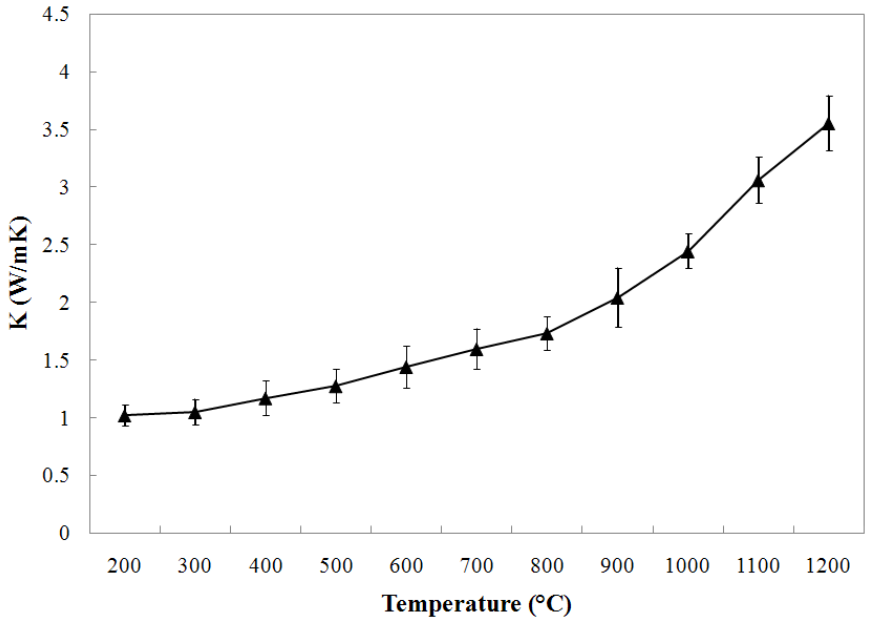

Figure 3.15 Thermal conductivity of the silica + zircon shell prepared at Missouri S&T foundry (fired at 900°C) by the laser flash test

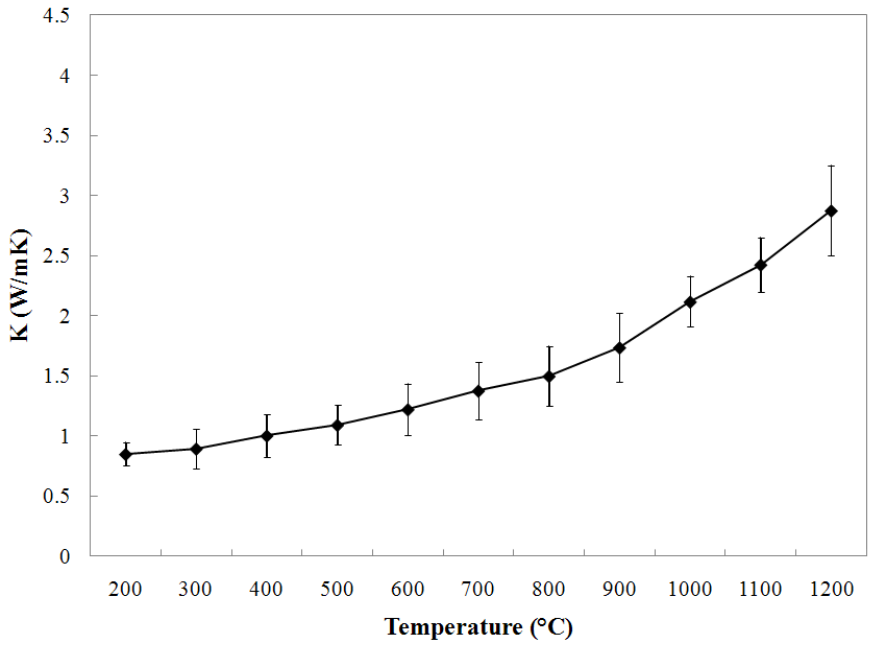

Figure 3.16 Thermal conductivity of the silica + aluminosilicate shell prepared at Missouri S&T foundry (fired at 900°C) by the laser flash test

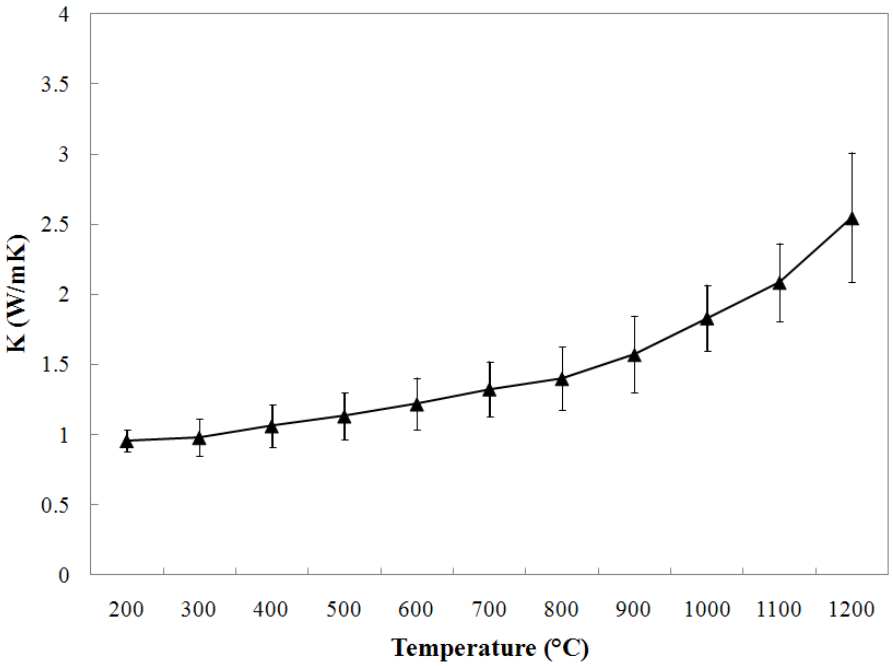

Figure 3.17 Thermal conductivity of the shell (fired at 900°C) measured for foundry A (flour – zircon, stucco – aluminosilicate) by the laser flash test

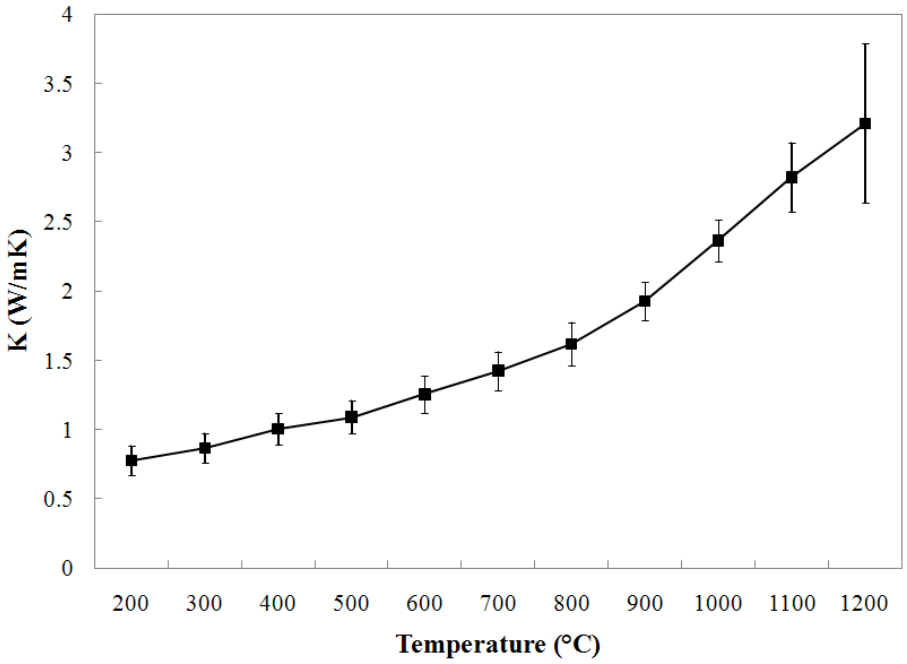

Figure 3.18 Thermal conductivity of the shell (fired at 900°C) measured for foundry B (completely fused silica based) by the laser flash test

3.5. DISCUSSIONS

High temperature thermal properties of the ceramic shells that were studied were compared to the properties of pure refractory materials.[33] There is considerable difference between C_p and K of pure materials used for shell building and the shells prepared from it. The C_p and K data of pure materials are of zero porosity. While ceramic shells prepared from pure refractory materials have complex structure. Parameters like binder content, surfactants, method of stucco application, closed and open porosity and sintering can have a significant effect on C_p and K. Also the layered structure which is produced affects K.

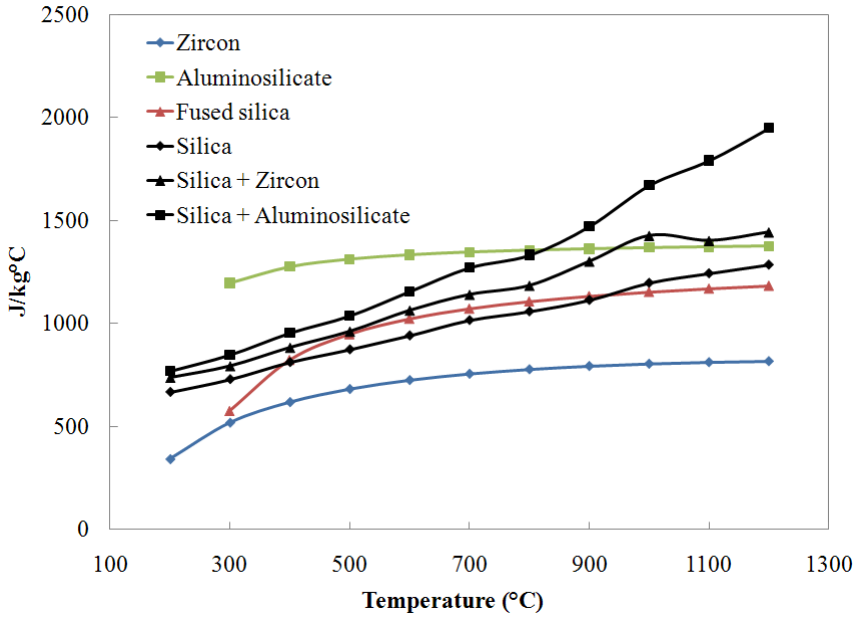

Figure 3.19 Comparison of specific heat capacity data for pure refractory materials obtained from Factsage (Fused silica, aluminosilicate-kyanite) with the data obtained from laser flash test for the shells prepared at Missouri S&T fired at 900°C

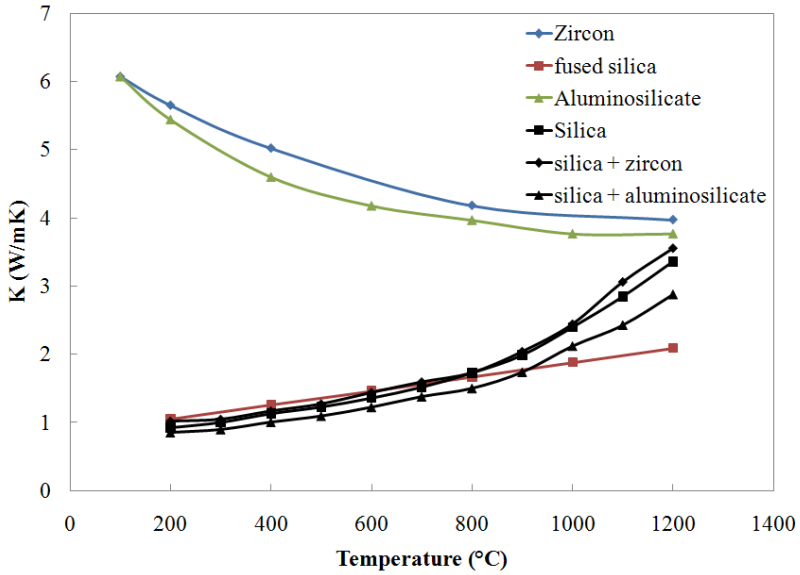

Figure 3.20 Comparison of thermal conductivity data of pure refractory materials [33] with the data obtained from laser flash test for the shells prepared at Missouri S&T fired at 900°C

The heat capacity of fused silica based shells showed a similar trend to pure silica. The C_p value increased with increase in temperature. The silica + zircon shells had C_p values higher than pure materials of both forms. For silica + aluminosilicate shells, it was observed that C_p values were higher than pure aluminosilicate. Foundry A and foundry B used different shell formulations which produced different values of heat capacities. Both foundry A and foundry B had same firing history.

For fused silica based shells, the one prepared at Missouri S&T as well as foundry A had *K* values higher than pure fused silica. Pure zircon and aluminosilicate have higher thermal conductivity than silica and decreases with increasing temperature. For shells prepared from these materials, it was observed that thermal conductivity increases with temperature. The highest measured *K*-values of silica + zircon and silica + aluminosilicate shells (having 40 to 50% fused silica in their structure) were still less than thermal conductivity of pure zircon and aluminosilicate at that temperature.

Changes in the heat capacity of the fired shell can be explained using silica phase transformation [34, 35] data. At atmospheric pressure, α-quartz will transform to hexagonal β-quartz at 573°C, upon further heating it will transform to hexagonal β-tridymite at 870°C and then to β-cristobalite at 1470°C and at 1705°C it melts (Figure 3.21-route a). However tridymite does not form from pure β-quartz unless certain amounts of trace elements are added (Figure 3.21-route b). The process (Figure 3.21-route b) is reversible if the temperature changes are slow. If quartz crystal is heated quickly then α-quartz will get converted to β-quartz but after that β-quartz will directly melt. The stability of β-quartz is less than β-cristobalite at melting temperature and hence its crystal structure is easily broken up (Figure 3.21-route c).

If melted silica is cooled fast then it gets converted to amorphous silica glass (Figure 3.21-route d). When silica glass is heated it skips the transition to *β*-quartz, *β*-tridymite and gets converted to *β*-cristobalite and at 1705°C it melts.

From figure 3.11 and 3.12 in the first run of the samples, a drop in Cp was observed after 1000°C. In figure 3.13 it was not observed since shell was already fired to 1200°C and already transformed to β-cristobalite at 1000°C during firing. If polymorph β-cristobalite is cooled quickly its crystal structure is preserved and will transform to α-cristobalite at 270°C. This transformation is reversible. In figure 3.11 and 3.12, during the second run transformation of α-cristobalite to β-cristobalite is clearly observed indicated by the peak after shell samples had reached 1200°C during first run. For the shell fired to 1200°C this transformation was observed in both runs. However the shell structure after 1200°C is not 100% cristobalite. Previous XRD work at Missouri S&T had shown there are trace amounts of trydimite present in the shell which may have a significant effect in Cp value and could be cause of decrease in the Cp value observed in first run of figure 3.11 and 3.12. This is subject of future work going on in Missouri S&T.

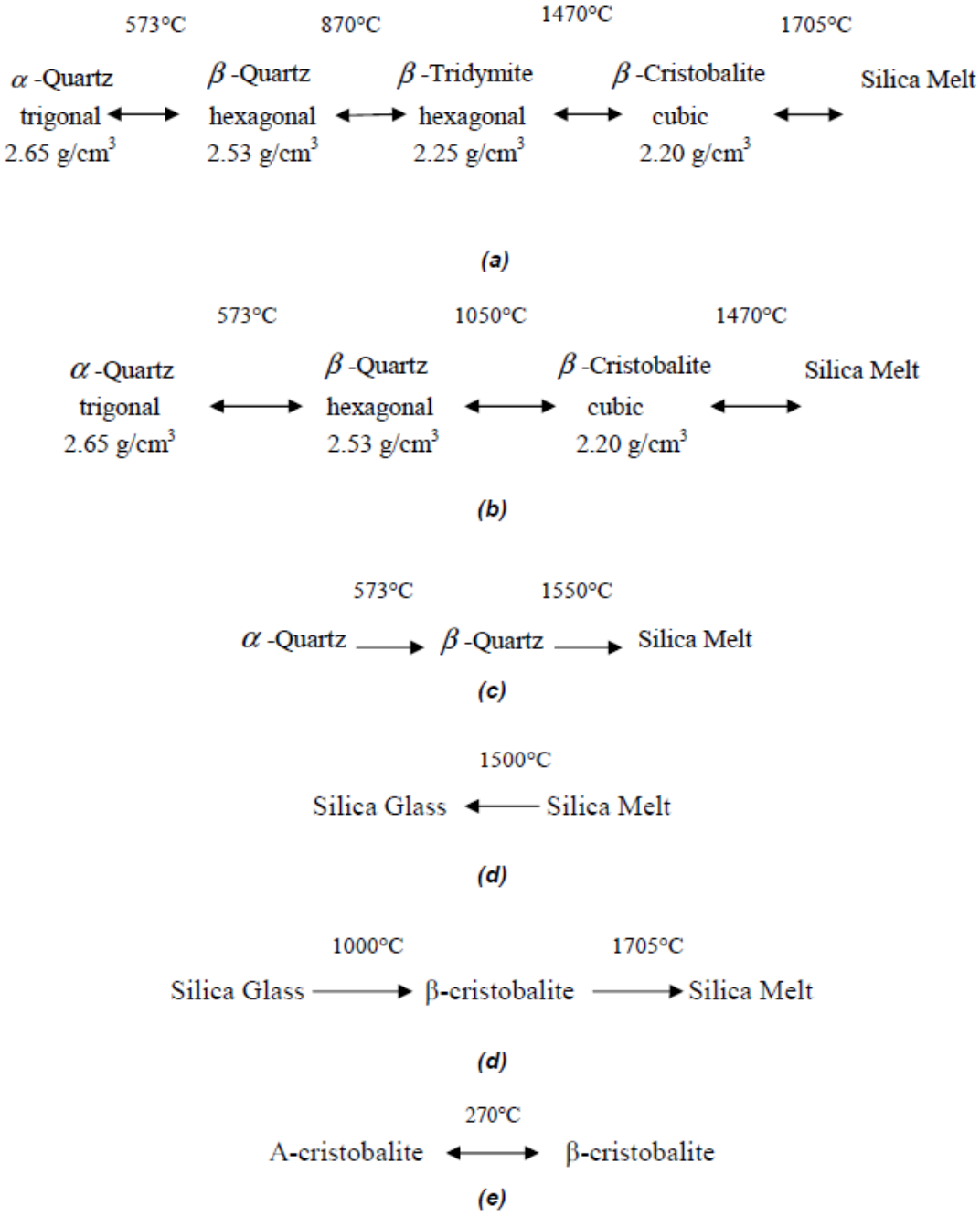

Figure 3.21 Possible phase transformations [34] in silica shells

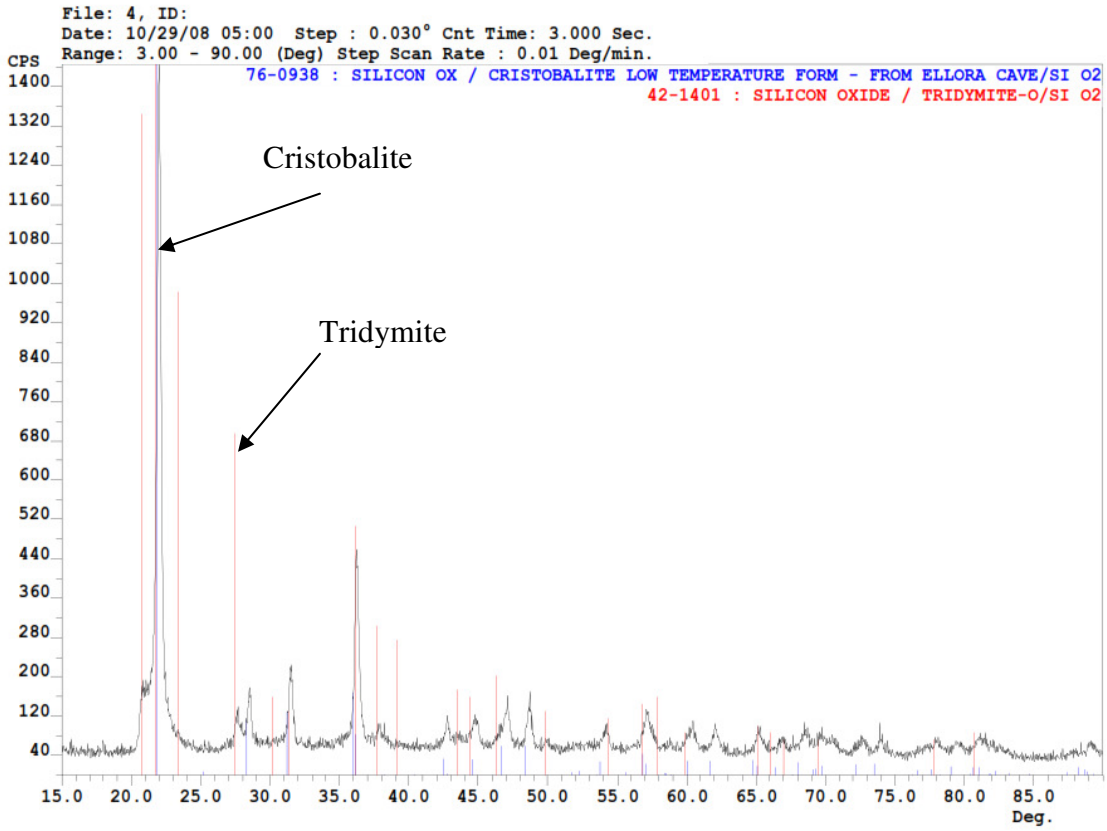

Figure 3.22 Presence of cristobalite and tridymite in the shell fired to 1200°C [36]

From Figure 3.11 in the first run of the samples, a drop in C_p was observed after 1000°C. In Figure 3.13, this drop in C_p was not observed since shell was already fired and already transformed to β-cristobalite during firing. If polymorph β-cristobalite is cooled quickly its crystal structure is preserved and will transform to α-cristobalite at 270°C. This transformation is reversible. During the second run transformation of α-cristobalite to β-cristobalite is clearly observed. Hence for solidification modeling, if the shells are already fired to 800°C and then preheated to 800°C again just before pouring *Cp* values can be assumed from figure 3.12 following the curve from point A to point D.

Figure 3.23 and Figure 3.24 show the databases developed in Magmasoft for different type of Investment casting shells.

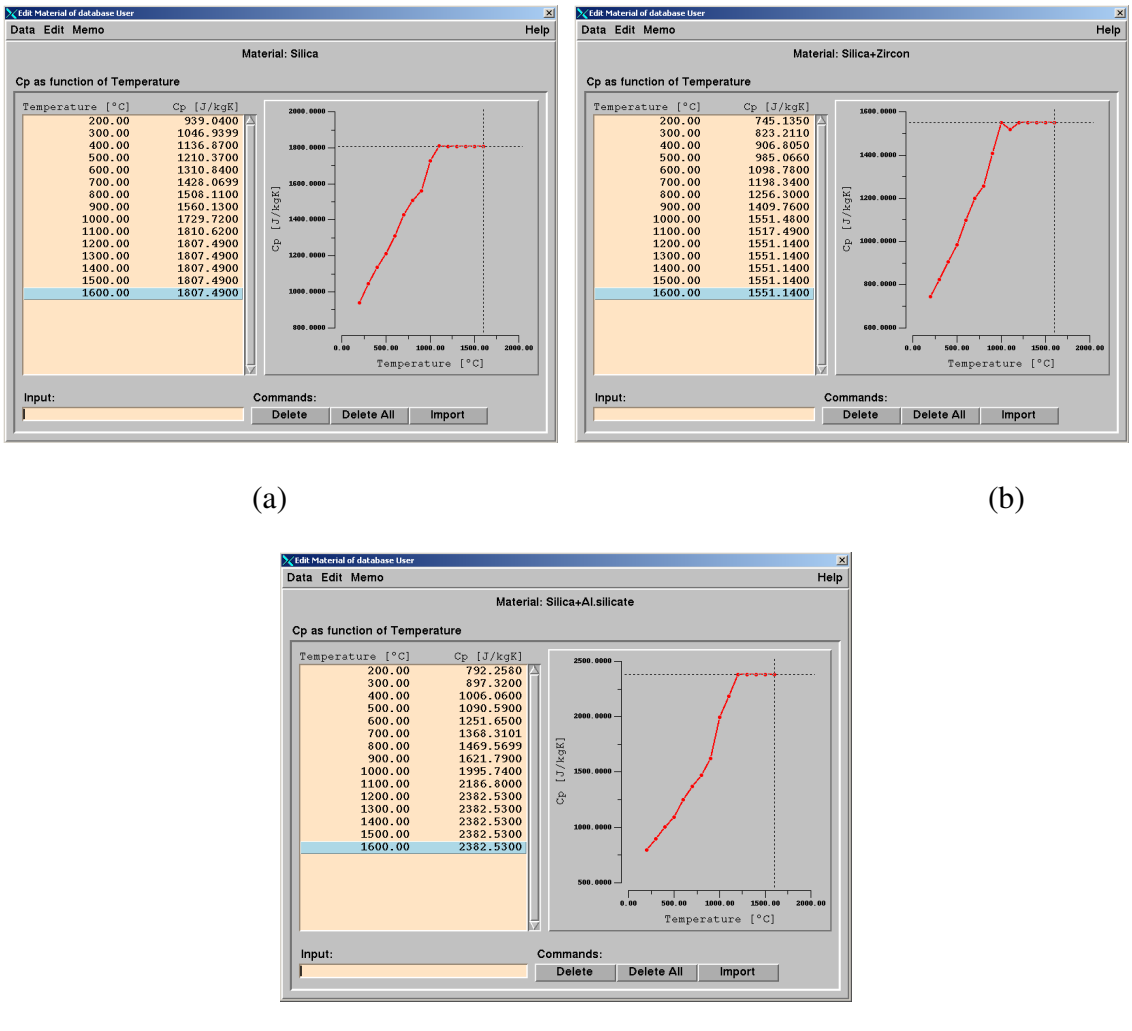

(a) (b)

(c)

Figure 3.23 Specific heat capacity database shown in Magmasoft for (a) fused silica based shells, (b) silica + zircon based shells, and (c) silica + aluminosilicate based shells.

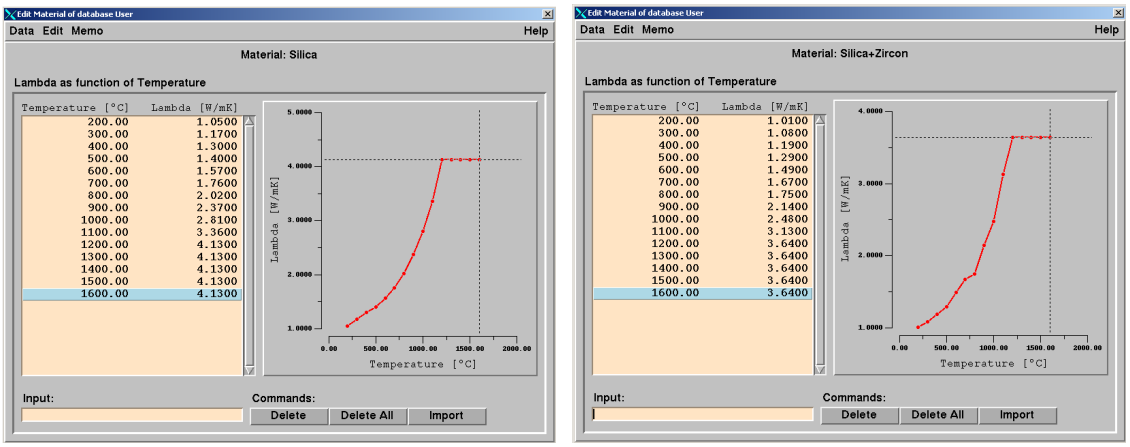

(a) (b)

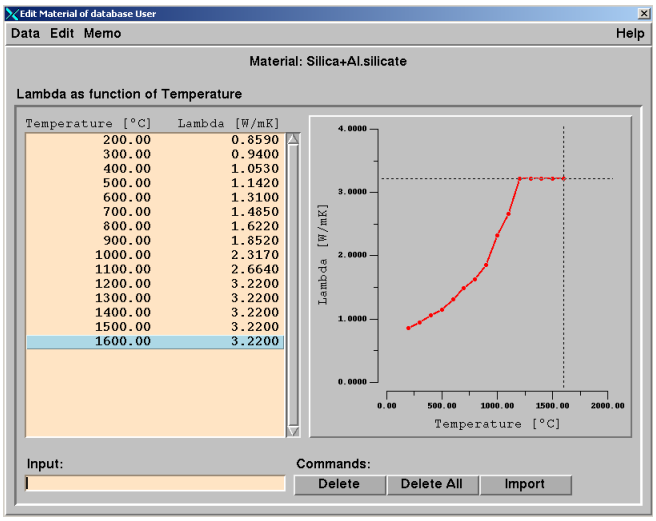

(c)

Figure 3.24 Thermal conductivity database shown in Magmasoft for (a) fused silica based shells, (b) silica + zircon based shells, and (c) silica + aluminosilicate based shells.

3.6. CONCLUSIONS

The thermo-physical properties of investment casting shells at high temperatures were successfully measured using the laser flash test and differential scanning calorimetry. A ceramic shell database for simulation software (Magmasoft) was developed.

The composite structure of the shell was observed to behave in a significantly different manner when compared to the data of pure refractory materials used for the shell building process. Parameters such as binder content of the shell, total amount of open and closed porosity and thermal history of the shell (pattern removing, firing, preheating temperatures) can have significant effect on thermal conductivity and specific heat capacity of investment casting shells due to fused silica phase transformations. The displacive transformations of fused silica have an important influence during pattern removal and breakout of the molds in investment casting.

3.7. FUTURE WORK

In future work for measurement of thermal conductivity of investment casting shells a new approach will be tested with two different methods, a single thermocouple method and an inverse method using two thermocouples.

In the single thermocouple method, solidification parameters will be determined for unknown steel solidified in known ceramic mold. For the inverse method two thermocouples will be inserted, one to measure the temperature of the steel and the other inside the shell. In this case the thermal properties of the unknown ceramic mold can be determined by pouring a metal with known properties like nickel etc.

Further measurements with laser flash test and DSC will be continued and compared with the new methods developed.

4. LIQUID STEEL-CERAMIC SHELL INTERACTIONS IN INVESTMENT CASTING

After the investment casting molds are poured, during the break out of the molds, difficulty in removing shell from the pocket regions of a casting is observed. In the investment casting industry, high pressure air, pressurized water jets, shot blasting, solution bath and other methods are used to remove shell materials attached to castings.

During a previous project at Missouri S&T, a complex geometry casting of approximately 150 lb was cast at an industrial foundry. Before cutting the casting it was necessary to remove the shell from the pocket regions. Attempts were made with high pressure water jets, and were not successful to remove it. Hence a small piece of steel in contact with ceramic was cut from the castings, polished and analyzed using SEM/EDS. Reaction products were observed deep inside the ceramic shell. Figure 4.1 shows examples of the interaction products observed. When steel is poured into preheated ceramic shells, the prime coat of the shells comes in contact with the melt and its oxides. Thus, there is the possibility of melting and/or chemical reactions at the mold-metal interface. This phenomenon has not been investigated in detail in the investment casting industry. However, prevention or reduction of interaction products could be beneficial in reducing scrap, cleaning and finishing costs. Hence it was decided to study liquid steel-ceramic shell interactions in detail with pattern design, Magmasoft simulations, thermodynamic predictions and SEM/EDS analysis.

During setting goals of the project it was found that three industrial foundries were interested in studying the same phenomenon. Hence it was decided to compare the results of shells prepared at Missouri S&T foundry with industrial shells.

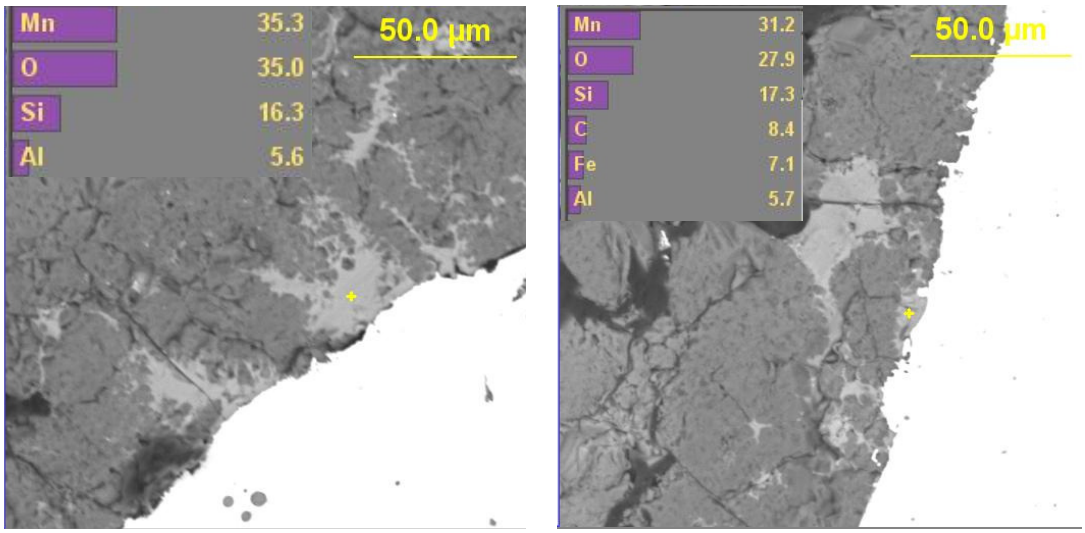

Figure 4.1 Reaction product (Mn-Si-O) penetrating inside ceramic shell

4.1. PATTERN DESIGN

Industrial trials of large complex castings showed that ceramic shell material in the deep pocket regions adjacent to heavy sections of the castings is most difficult to remove during break out of the shell molds. Hence it was necessary to study the interaction products in this type of region. A special 4”x4”x6” specimen with a cube-shaped internal cavity having ½” side wall thickness and 1½” bottom thickness was designed as shown in Figure 4.2. The vertical downsprue was attached to the bottom of the cube. A vent was attached to prevent gas entrapment and fill the shells completely during the pour.

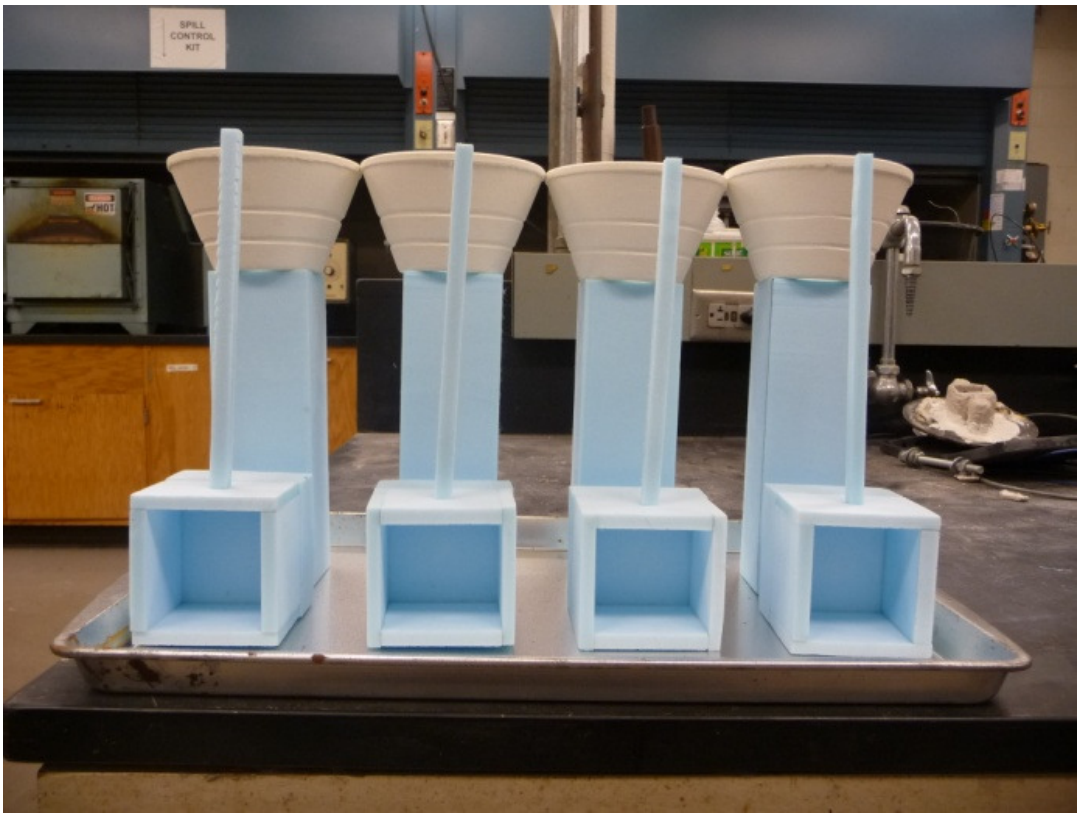

Figure 4.2 Foam Patterns

4.2. MAGMASOFT SIMULATIONS

Magmasoft software was used for simulation to design the experiment. To determine the temperature history in the prime and the backup coats as well as in casting, three control points were placed in the shell and one was placed in the casting near the corner of internal pocket as shown in Figure 4.3 and 4.4. The one in the casting denotes the temperature of the solidifying steel and the other three monitored temperature in the prime and back up coats at points placed 0.5 mm, 3 mm, and 6.5 mm from casting surface respectively.

User defined thermal property databases [37] were created for steel (HY130) and fused silica based investment casting shell. A fine mesh was selected for the shell to

accurately predict the temperature at the control points. The simulation was started at a pouring temperature of 1650°C with shells preheated to 800°C and ran until the casting was completely solidified.

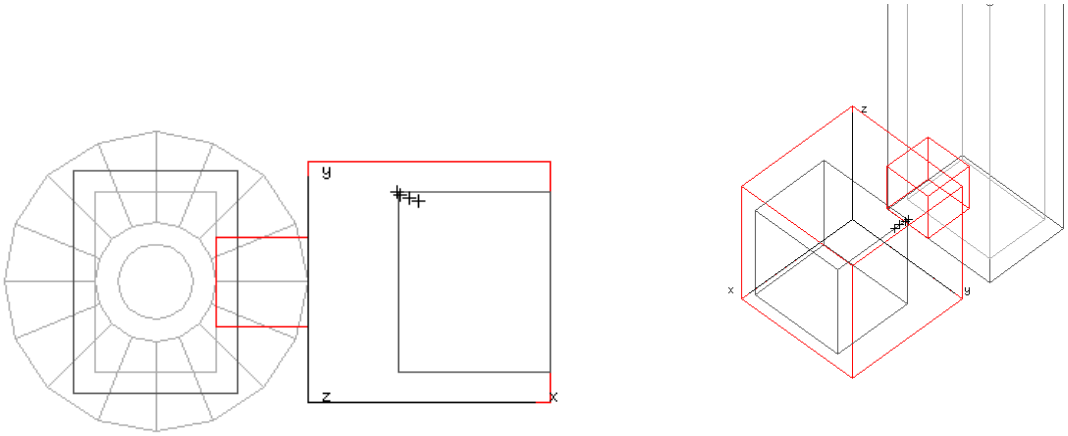

Figure 4.3 Control points

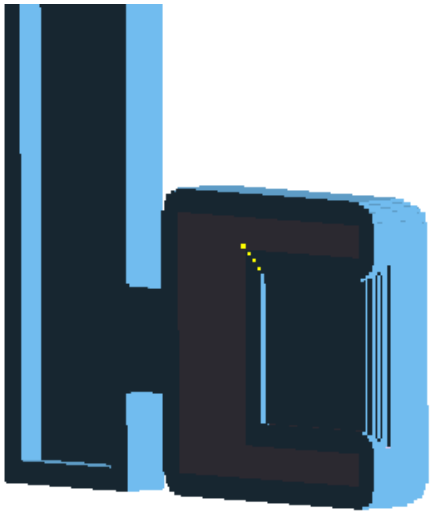

Figure 4.4 Cross sectional view of the shell

Simulation results predicted that the temperature of the prime coat of the shell goes above the liquidus temperature of the steel in the pocket region while the adjacent casting region still has some amount of liquid phase. The combination of these conditions increases the probability of steel-shell interactions in the internal pocket region being studied. Figure 4.5 shows the temperature distribution at 100% fraction solid steel in the casting which shows that the internal corners remain at high temperatures. Figure 4.6 shows the temperatures of the shell at selected control points during steel solidification.

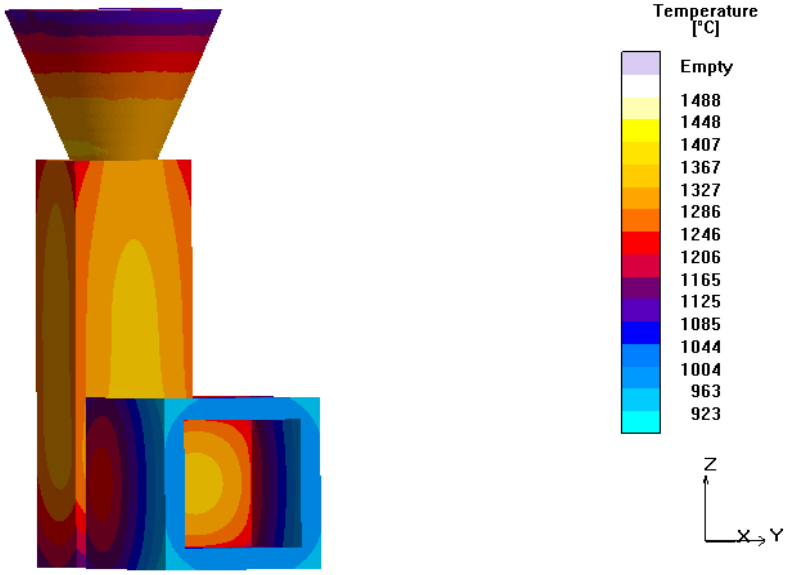

Figure 4.5 Temperature distribution at 100% fraction solid which shows that the internal corners remain at high temperatures

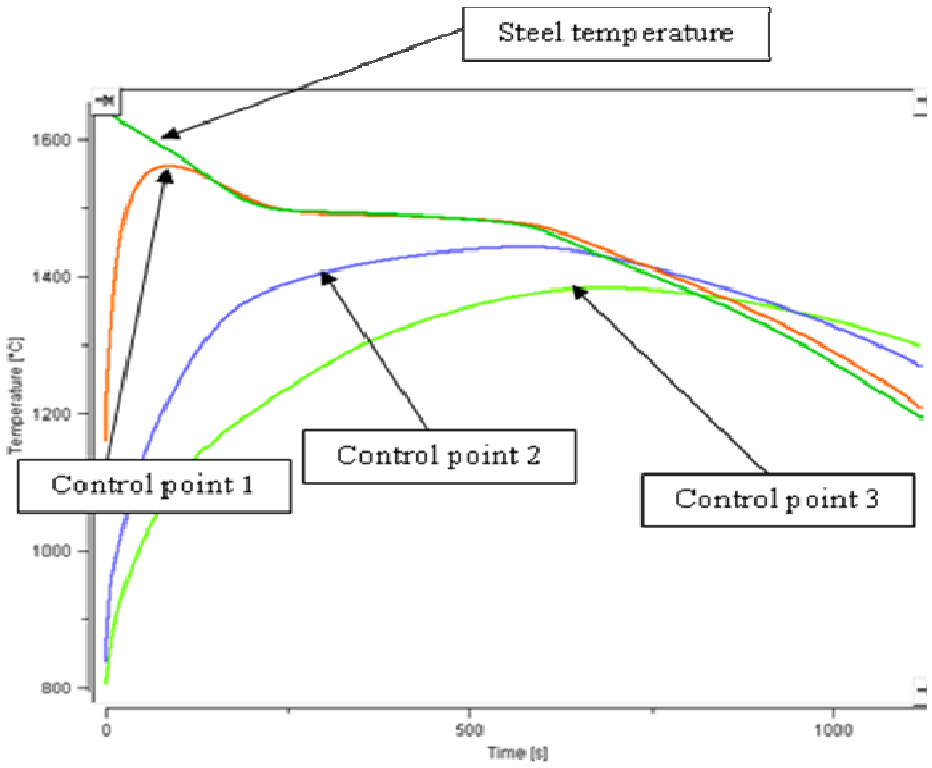

Figure 4.6 Temperature histories for control points at the corner of the casting and at 0.5(control point 1), 3.5 (control point 2) and 6 mm (control point 3) from the casting surface inside the ceramic shell during steel solidification

4.3. FACTSAGE MODELING

A thermodynamic model of liquid HY130 steel in equilibrium with the prime layer (solid phase), and a limited amount of oxygen (gas phase) was used to study the possible formation of a slag layer (liquid phase) on the steel. Thermodynamic modeling was done using FactSage software to study the amount and compositions of the possible liquid products of the reaction. Fact-Felq, Fact-Stel and Fact 53 databases were selected. Preliminary calculations showed that pure steel does not react with pure oxides in the shell at pouring temperatures in an inert gas atmosphere. The possible liquid products on

the metal – ceramic mold interface can be formed when the atmosphere contains oxygen. Calculations for this case were done in two steps. In step one, the equilibrium composition of the slag phase formed on the liquid steel surface in contact with 1.5% O_2 was calculated. The second model was run considering the reaction of the liquid reoxidation product (slag) formed in step one, with the solid prime coat material (silica, zircon, or alumina) to predict any liquid/solid product formation.

4.4. SHELL PREPARATION

Three types of shell with different prime coats were prepared in Missouri S&T Foundry. Dipping slurries for the prime coat were made of colloidal silica binder. The binder was mixed with one of three different types of 200 mesh flour: silica, zircon and alumina. These are referred to as silica, zircon and alumina prime coats. Fused silica stucco (50-100 mesh) was applied directly on the prime coat in all cases. All of the other five coats used the fused silica based slurry with the same colloidal silica as binder. 30-50 mesh silica stucco was used for these coats. Finally, one seal coat was given to all shells. Table 4.1 summarizes shelling procedure of three types of shells made at Missouri S&T.

In addition, shells prepared around the same pattern were obtained from three different commercial foundries A, B, C. Foundry A had zircon based prime coat and aluminosilicate as the stucco in the back up coats. Foundry B had the fused silica based prime coat and coarser mesh silica stucco in the back up coats. Foundry C had zircon based prime coat and silica as the stucco in the back up coats. All the shells were fired to 900°C for 3 hours at Missouri S&T Foundry. Figure 4.7 shows the shells prepared at Missouri S&T and castings after pouring.

Table 4.1 Investment casting shells prepared at Missouri S&T foundry

	Silica Shells	**Zircon Shells**	**Alumina Shells**
Prime coat Stucco	Slurry – (Fused silica + Binder) (2:1) Silica 100-200 mesh	Slurry – (Zircon flour + Binder) (2:1) Silica 100-200 mesh	Slurry – (Alumina flour + Binder) (2:1) Silica 100-200 mesh
4 Back up coats Stucco	Slurry – (Fused silica + Binder) Silica 30-50 mesh	Slurry – (Fused silica + binder) Silica 30-50 mesh	Slurry – (Fused silica + binder) Silica 30-50 mesh
Seal coat Stucco	Slurry – (Fused silica + Binder) -	Slurry – (Fused silica + Binder) -	Slurry – (Fused silica + Binder) -
% Open porosity	13.64	12.15	14.08

Table 4.2 Shells obtained from the commercial foundries

	Foundry A	Foundry B	Foundry C
Prime coat	Zircon based	Fused silica based	Zircon based
Back up coats stucco	Aluminosilicate	Silica	Silica
% Open porosity	21.57	17.86	17.96

(a) (b)

Figure 4.7 (a) Missouri S&T shells before pouring (b) castings after pouring

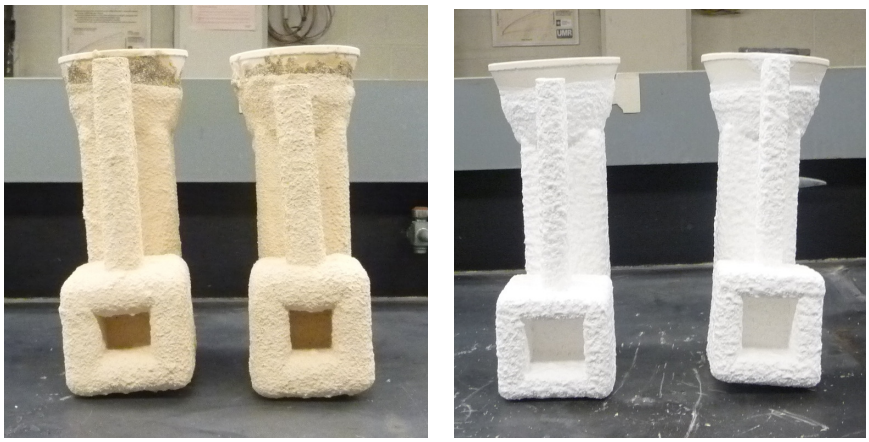

(a) (b)

(c)

Figure 4.8 Industrial shells: (a) foundry A (b) foundry B (c) foundry C

Figure 4.8 shows shells obtained from industrial foundries. The box-shaped part of the shells was covered with kaowool (Figure 4.9) in order to keep it at high temperature after pouring. Low carbon alloy steel (HY130) was melted in 100 lb induction furnace. A cover of argon gas was maintained on top of the melt to prevent reaction of liquid steel with atmosphere. Shells were preheated to 800°C before pouring. Melt was poured into the ladle and deoxidized using 0.06% aluminum followed by 0.06% Ca-Si wire. Two heats were conducted. Shells prepared at Missouri S&T foundry were poured in first one and industrial shells in second one. Chemistries of the HY130 steel in two heats are shown in Table 4.3

Figure 4.9 (a) Shells coated with kaowool and (b) preheating in kiln

Table 4.3 Chemistry of HY130 steel in two heats poured at Missouri S&T

	C	Si	Mn	Cr	P	S	Ni	Al
Heat 1	.17	.31	.52	.63	<.001	.005	4.1	.06
Heat 2	.17	.31	.50	.64	<.001	.006	4.1	.06

After the castings had solidified, the shells were knocked off except from the pocket region. Figure 4.7 (b) shows the castings with ceramics intact in the pocket regions of cube castings. Mixture of epoxy resin and hardener was poured in these pockets and kept for 10 hours to get it hardened. Epoxy helped to keep the ceramic shell in contact with steel during sample preparation. After being stabilized by the epoxy the samples of the steel/ceramic shell interface were cut from the pocket region and mounted again in epoxy in order to have the specific sample size for ESM/EDS analysis. Samples were then polished from 180 to 800 grit SiC paper and after that they were polished with diamond paste 3, 1 and ½ micron using low speed cutting fluid. Samples were then carbon coated to decrease electrical charging under scanning electron microscope (SEM). SEM/EDS ASPEX PICA-1020 system (Particle Identification and Characterization Analyzer) was used to observe interaction products.

4.5. RESULTS

4.5.1. Silica Prime Coat Shells. Figure 4.10 shows the interaction products observed for silica prime coat shells. *Al-Si-Mn-O* phases were observed at the exact corner region (in the right angled portion). SEM images clearly show their penetration into the shell. *Fe-Si-Mn-O* phases were observed near the corner region but slightly away from it. Figure 4.10 shows that the reaction products had no penetration in steel and were located on the shell side. *Al-Si-Mn-O* phases had more tendencies to penetrate when compared to *Fe-Si-Mn-O* phases. Open porosity measured by the Archimedes method was 13.5% for the silica prime coat shells. (Appendix – table 3)

4.5.2. Alumina Prime Coat Shells. Figure 4.11 shows reaction products observed for alumina prime coat shells. *Al-Si-Mn-O* phases were observed at the exact corners similar to the silica prime coat shells. It can be seen in Figure 4.11 that they have penetrated more into the shell than silica prime coat shells. *Fe-Si-Mn-O* phases were observed slightly away from the corner and in some cases they can be seen at the higher depths into the shell. Open porosity measured by the Archimedes method was 12% for the alumina prime coat shells. (Appendix – table 3)

4.5.3. Zircon Prime Coat Shells. Figure 4.12 denotes the interaction products observed for the shells with zircon prime coat. *Fe-O-Zr-Si* products were observed which showed there has been some melting of the prime coat at the interface. These phases were observed only near the contact surface between casting and shell. Another type of product observed distinctly was *Mn-Si-Al-O* phase which was in the corner region. This phase was found near surface and also inside the prime coat (Figure 4.12 - b). Open porosity measured by the Archimedes method was 14% for the zircon prime coat shells.
(Appendix – table 3)

4.5.4. Industrial shells (foundry A, B & C). Figures 4.13-4.15 show the interaction products observed for industrial foundry shells, foundry A, B and C respectively. Similar to results observed for the Missouri S&T shells *Al-Si-Mn-O* products were observed to be present at the corners for foundry A and B with foundry B showing greater penetration into the shell. *Fe-Si-O-Mn* products were observed in the samples from of all three foundries with the maximum penetration in foundry B. Foundry C samples showed least penetration into the shell.

During SEM analysis it was confirmed that the foundry A had zircon based prime coat and aluminosilcate as the stucco in back up coats. Foundry B had fused silica based prime coat and coraser mesh silica as stucco in the back up coats. Foundry C had zircon based prime coat and silica as the stucco in the back up coats. Archimedes method was used to obtain the data of percent open porosity in industrial shells. The percentages of open porosity found were, foundry A had 21.5%, foundry B had 18% and foundry C had 18%. (Appendix – table 3)

All industrial foundries showed some penetration of reaction products on the steel side. However this is a subject of future research at Missouri S&T. No surfactants, polymers were used for Missouri S&T shells and also binder content of the shells were very low. However it should be noted that higher binder and polymer content is important for green strength of the shell. Surfactants are important for wetting of the slurry to pattern (prime coat) and getting flour in to the slurry in a stable manner.

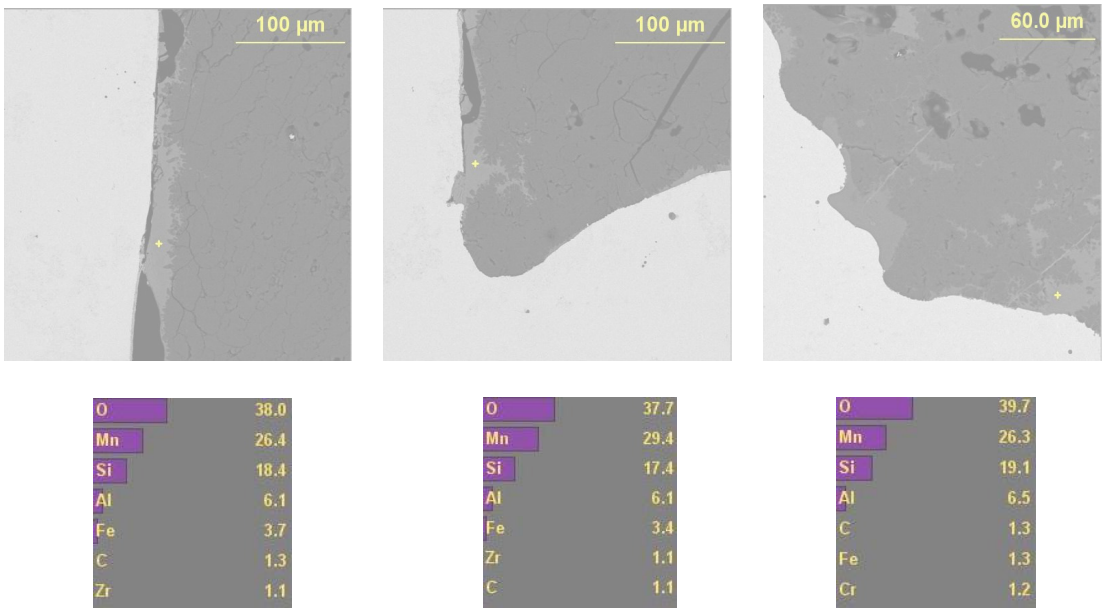

(a)

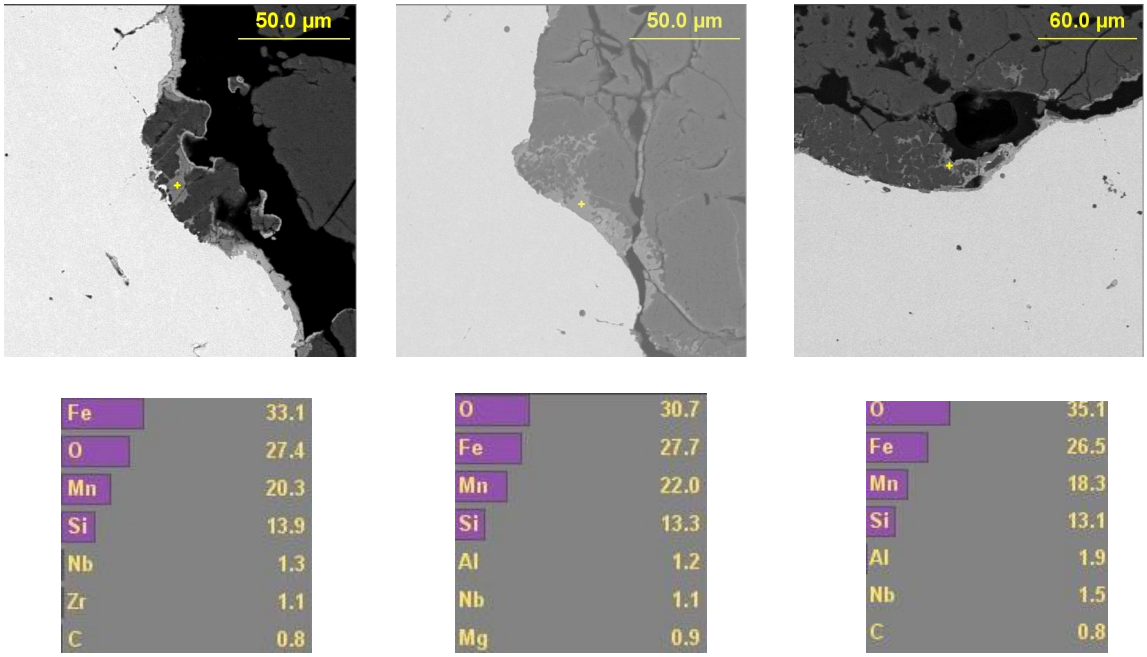

(b)

Figure 4.10 Silica prime coat shells interaction products (a) Al-Si-Mn-O and (b) Fe-Si-Mn-O phases

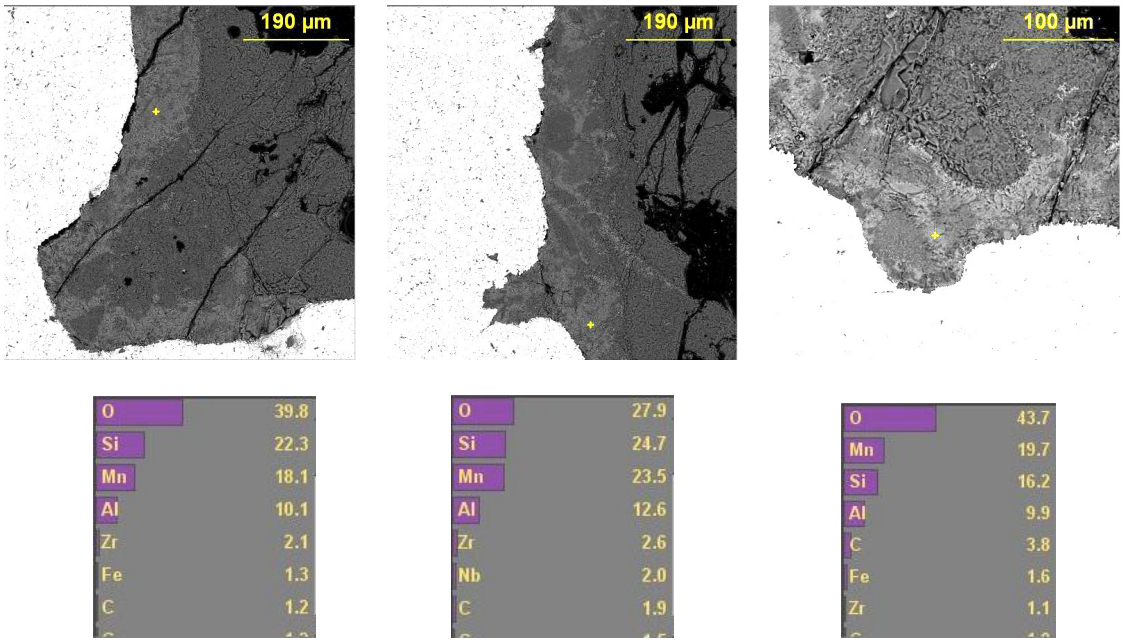

(a)

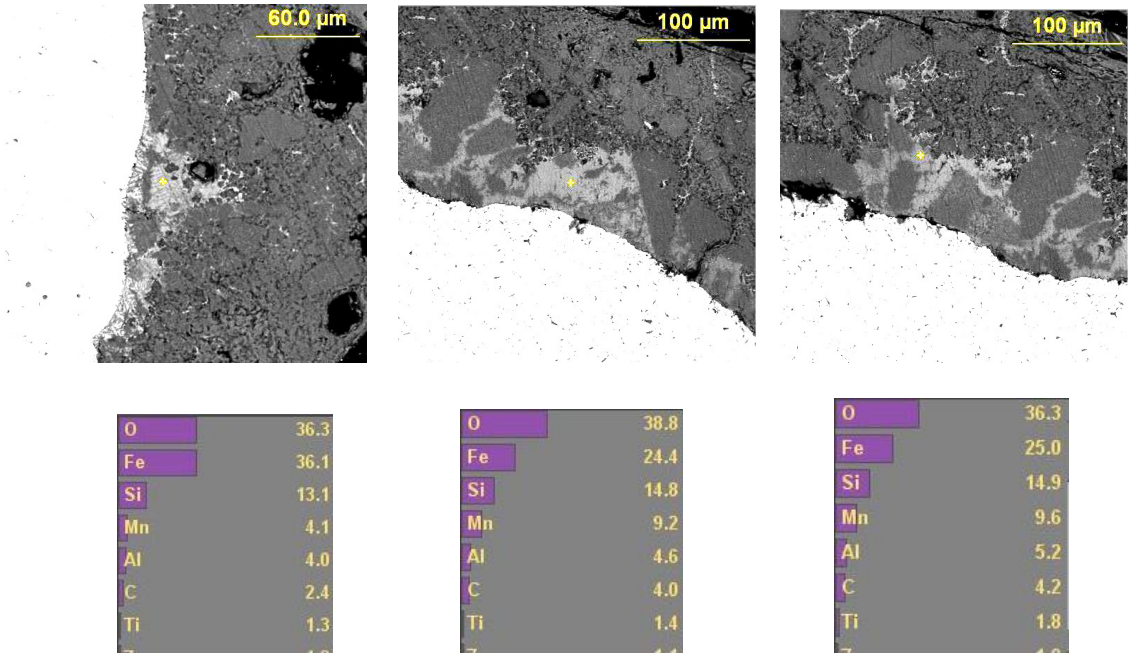

(b)

Figure 4.11 Alumina prime coat shells interaction products (a) Al-Si-Mn-O (b) Fe-Si-Mn-O

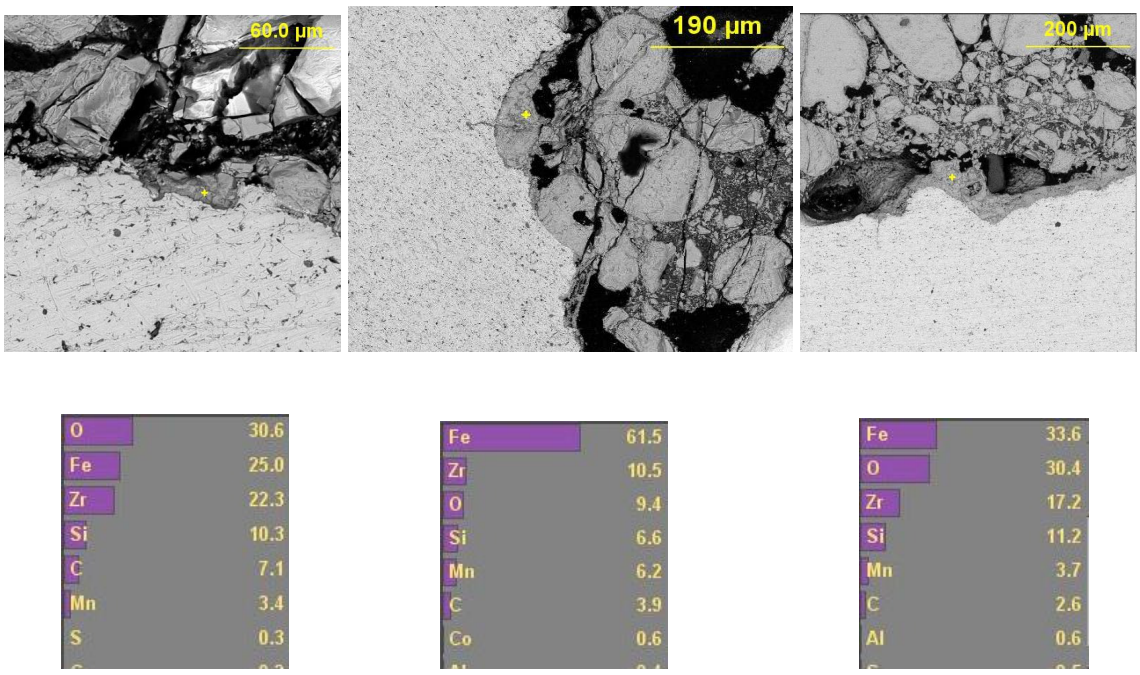

(a)

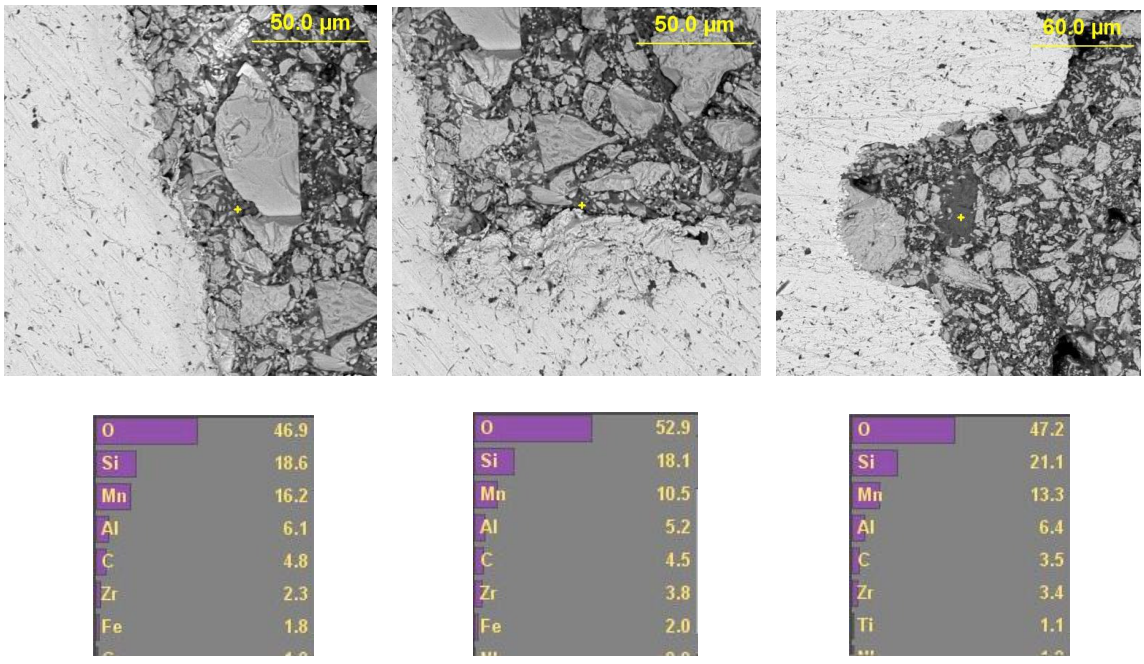

(b)

Figure 4.12 Zircon prime coat shells interaction products (a) Fe-Zr-O-Si (b) Al-Si-Mn-O

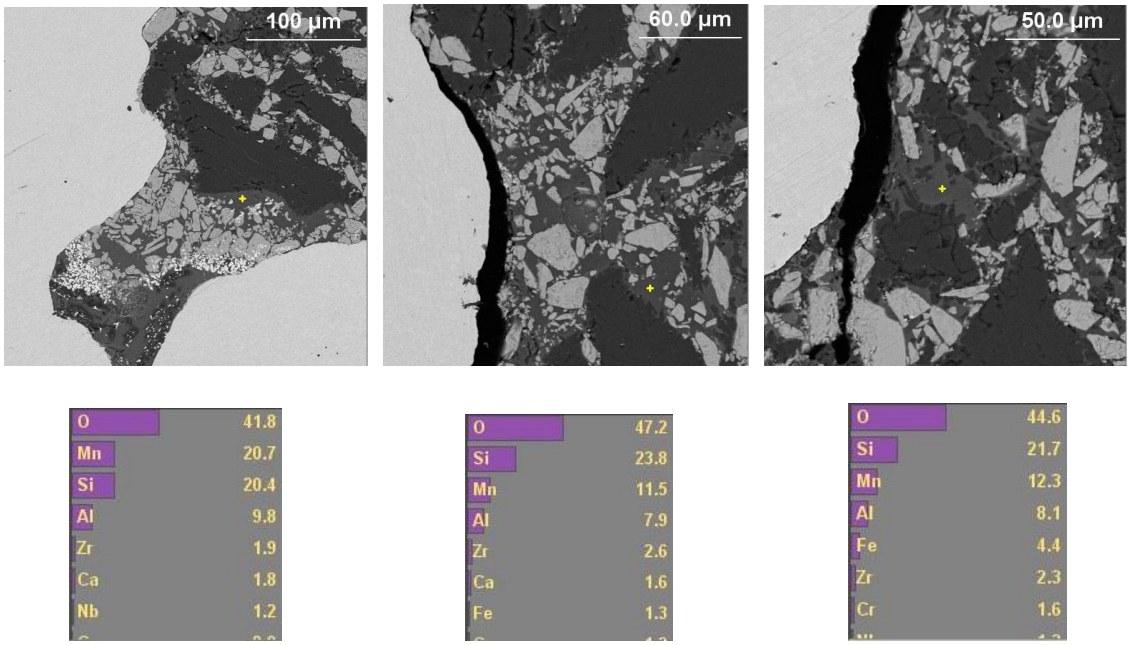

(a)

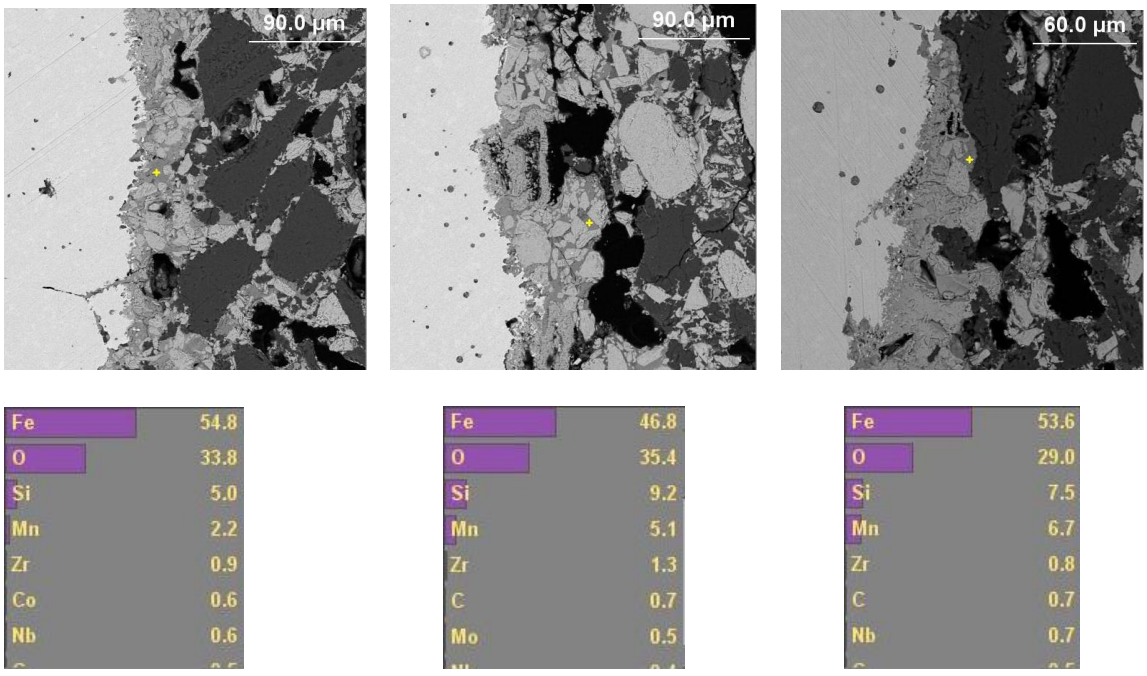

(b)

Figure 4.13 Interaction products Al-Si-Mn-O (a) and Fe-Si-Mn-O (b) phases observed in shell samples from foundry A

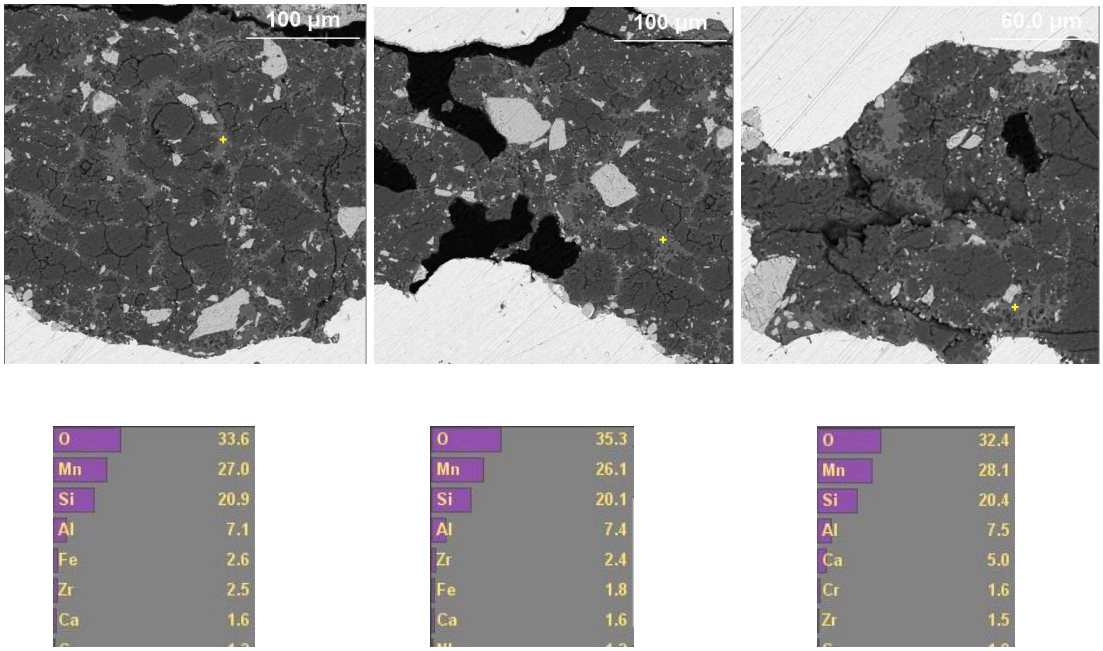

(a)

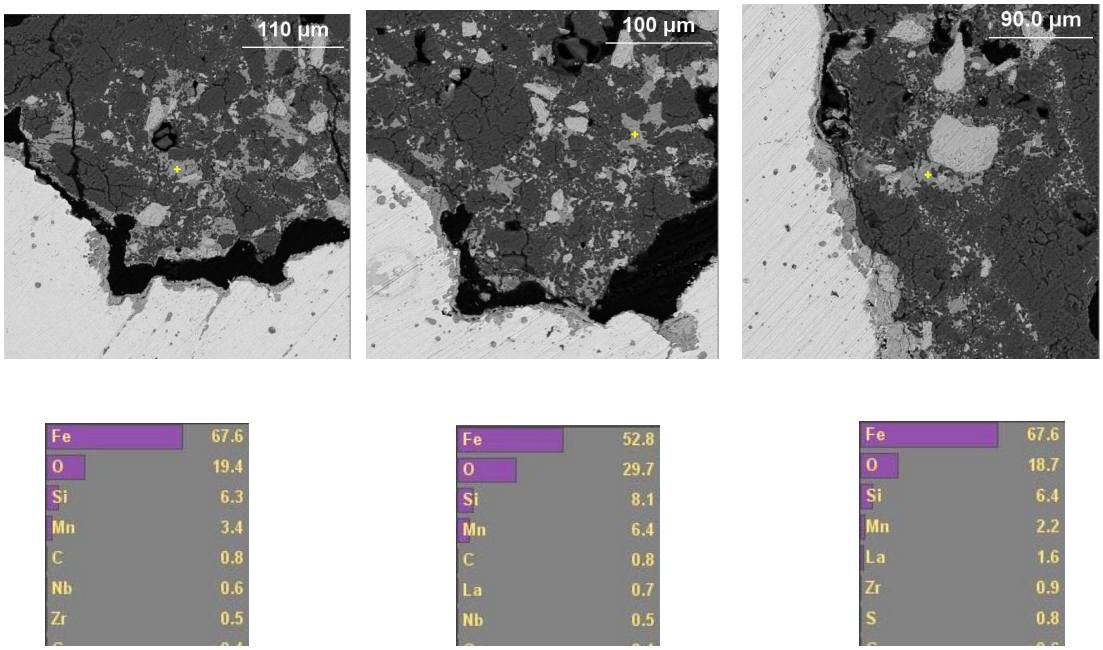

(b)

Figure 4.14 Interaction products Al-Si-Mn-O (a) and Fe-Si-Mn-O (b) phases observed in shell samples from foundry B

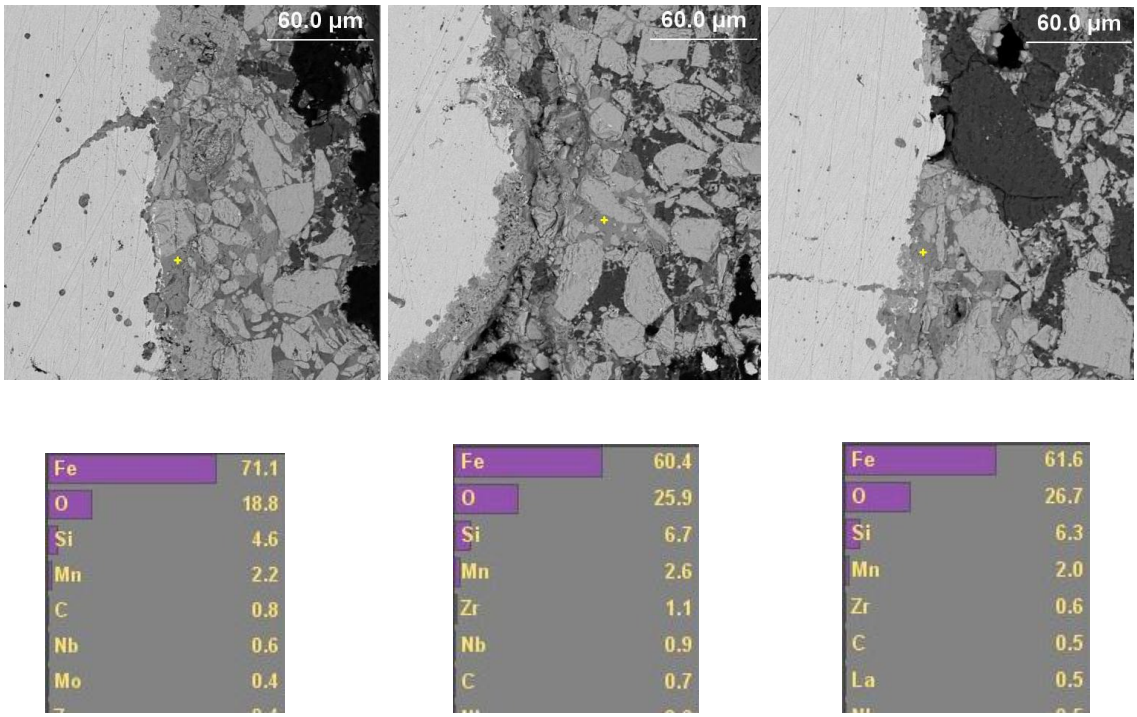

Figure 4.15 Interaction products Fe-Si-Mn-O phase observed in shell from foundry C

4.6. DISCUSSIONS

4.6.1. Thermodynamic predictions. Preliminary calculations from Factsage showed liquid steel (low and medium carbon) does not directly react with pure oxides (silica, alumina and zircon) at pouring temperatures in an inert atmosphere. When the atmosphere contains oxygen, steel will spontaneously react to form different reoxidation products. Reoxidation products were denoted as reoxidation product (slag) in this report. For the purpose of the thermodynamic modeling using Factsage, it is denoted as “slag” in the solutions menu.

4.6.1.1. Factsage first model. The first equilibrium model was run in Factsage to predict the possible reoxidation product (slag) composition which could be formed when the liquid steel comes in contact with the oxygen from the atmosphere during ladle transfers

and mold pouring. The reoxidation product on liquid steel surface will contain a mixture of oxides in the ratio of 40-50%*Si, 10-20%Fe, 20-30%Mn* with small amount of *Al* and *Cr* oxides. The reoxidation slag thus formed has a long solidification interval and could be liquid below the solidus temperature of steel (Figure 4.16). The reoxidation product (slag) also has high solubility for the shell component oxides. The main solid phases in the solidified slag (steel reoxidation product) are solid solution $(Fe_xMn_{1-x})SiO_3$ and solid solution mullite (Al_2O_3-SiO_2). This type of liquid reoxidation product (slag) can readily react with the prime coat during melt cooling and casting solidification in the shell.

4.6.1.2. Factsage second model. The second equilibrium model was run to predict the complex reactions which could take place between the reoxidation product (slag) and the solid prime coats containing silica, alumina or zircon. The main goal of these calculations was prediction of possible liquid products that could form with the prime coat at temperatures predicted from Magmasoft thermal modeling. If a predicted liquid reaction product has larger solubility of the solid ceramic it will indicate a higher severity of the possible metal/mold interaction. The predicted possible reaction products are shown in Table 4.4. The silica ceramic can readily react with the reoxidation product (slag) containing *Mn* and *Fe* oxides at steel pouring and solidification temperatures resulting in the formation of a liquid phase. This liquid phase has the possibility of dissolving a large amount of solid silica from the shell without solid precipitates. Reaction of reoxidation slag with alumina also creates a liquid phase region stable at steel pouring and solidification temperatures. Only the reaction of reoxidation slag with zircon produces a lower quantity of the stable liquid phase at 1550°C.

For the comparison of the possible behavior of the different prime coats (C) in contact with the liquid reoxidation product (S), the reactions between the reoxidation slag and the prime coats were analyzed with respect to the formed liquid product (D). The formation of the liquid product (D) indicates the dissolution of the prime coat in slag. Fig. 4.17 shows the equilibrium amount of the dissolved prime coat (D) versus initial reactant composition as S/(S+C). These thermodynamic calculations were done at maximum predicted temperature in the shell (1550°C). The alumina prime coat has significantly larder dissolved fraction D of the prime coat as compared to the zircon prime coat for the same amount of liquid slag S/(S+C).

Figure 4.17 also confirms that a pouring practice which controls the melt reoxidation will result in less volume of interaction products if the zircon prime coat shell is used. Steel reoxidation slag can dissolve significantly larger amount of silica and alumina prime coats when compared to the zircon prime coat. The experimentally observed chemistries of the phases in interaction regions were compared with the thermodynamically predicted reaction products and similarity was confirmed.

4.6.2. Possible steps involved in liquid steel - prime coat reactions

Possible steps responsible for liquid steel – prime coat reactions could be given as follows

1. Formation of steel reoxidation product (slag) on steel surface during pouring
2. Formation of liquid reaction products between the reoxidation product (slag) and the prime coat
3. Growth of the liquid interaction product and its penetration into the ceramic shell.

Table 4.4 Equilibrium model prediction for interaction products by Factsage

Reactions	**Interaction product**
Liquid steel reoxidation slag + SiO_2 prime coat	Liquid slag + SiO_2+ $(Fe_xMn_{1-x})SiO_3$ + mullite $(Al_2O_3\text{-}SiO_2)$.
Liquid steel reoxidation slag + Al_2O_3 prime coat	Liquid slag + Al_2O_3 + $(Fe_xMn_{1-x})SiO_3$ + mullite $(Al_2O_3\text{-}SiO_2)$.
Liquid steel reoxidation slag + $ZrSiO_4$ prime coat	Liquid slag + $ZrSiO_4$+ $(Fe_xMn_{1-x})SiO_3$ + mullite $(Al_2O_3\text{-}SiO_2)$.

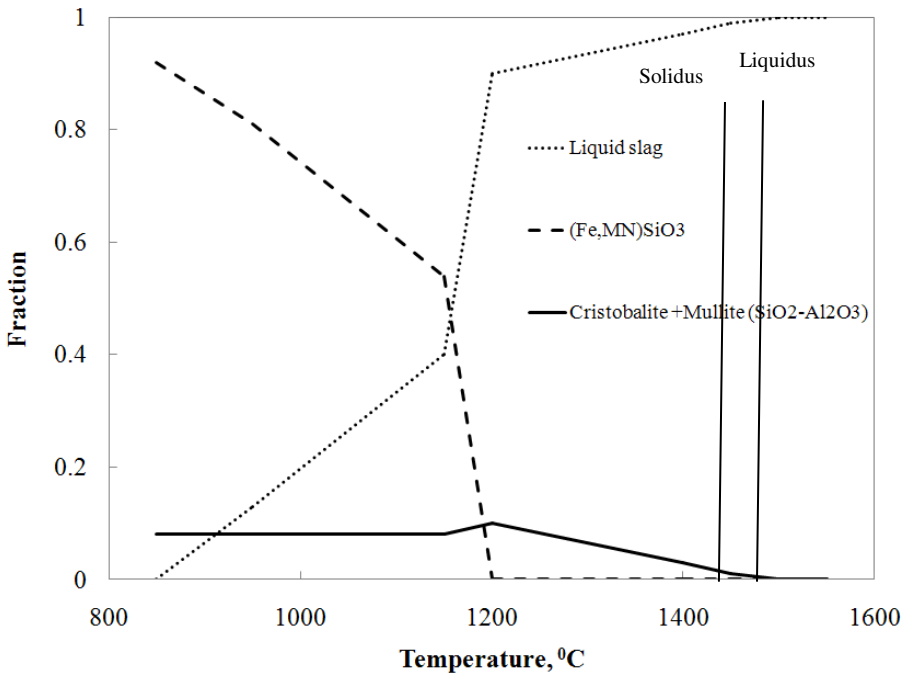

Figure 4.16 Solid phase formation during cooling reoxidation slag (Factsage).

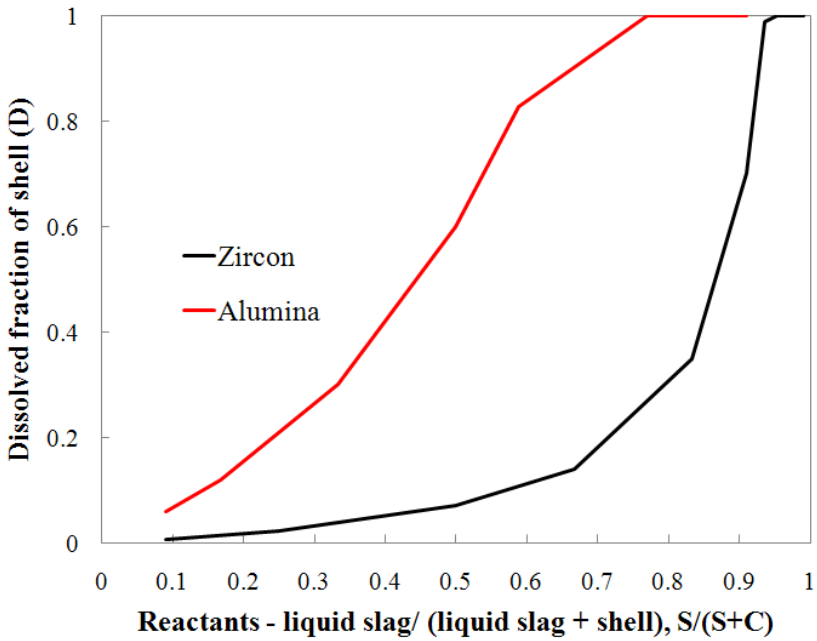

Figure 4.17 Equilibrium amount of the dissolved prime coat (D) versus initial reactant composition as S/(S+C) at 1550°C

The studied interaction products are the liquid solutions of oxides formed due to the reaction of the slag with the solid prime coat materials. The reoxidation product (slag) has a low melting temperature and could aggressively react with the prime coat if the temperature is sufficient for the reaction. The reoxidation product (slag) dissolves the prime coat. As a result the liquid reaction product and metal gains access to the more porous stucco layer that is very easy to penetrate because the pores are larger and the fraction porosity is higher. The best but most expensive way to prevent interaction product formation is to cast in vacuum or otherwise protect the pouring stream from reoxidation. Also some improvements could be made to limit active liquid steel reoxidation for regular air pouring practices. For example introducing a reducing/protection gas in the shell or removing oxygen from protection cover after

pouring can potentially help to prevent interaction product formation to a certain extent. Counter gravity pouring also can prevent steel reoxidation.

Pouring temperature also has an important effect on intensity of formation of interaction products. It is important to note, that reactions take place when shell temperature rises above steel solidification temperature. More superheat will result in a greater amount of liquid slag formed and the ceramic shell will be subjected to the temperatures above reoxidation product (slag) solidus for longer time. Hence care must be taken to minimize superheat before the shells are poured.

Casting geometry, for example deep pockets connected to hot spots in the casting body, can presumably have more surface reaction products. This will largely depend on the porosity of the prime coat. In investment casting amount of porosity of the prime coat is important because some level of porosity is necessary for overall shell permeability. If porosity is too high, there could be greater penetration of reaction product into the prime coat.

4.6.3. Depth of penetration of interaction products. It was observed that the amount of interaction products and their depth of penetration in the shell were higher for silica and alumina prime coat. For the shells with a zircon prime coat both interaction products and their depth were lower. Finally, Figure 4.18 show the maximum depth of reaction products in shells that were studied as a function of percentage apparent porosity. The varying results for the industrial shells were caused by a combination of varying prime coat composition and shell porosity.

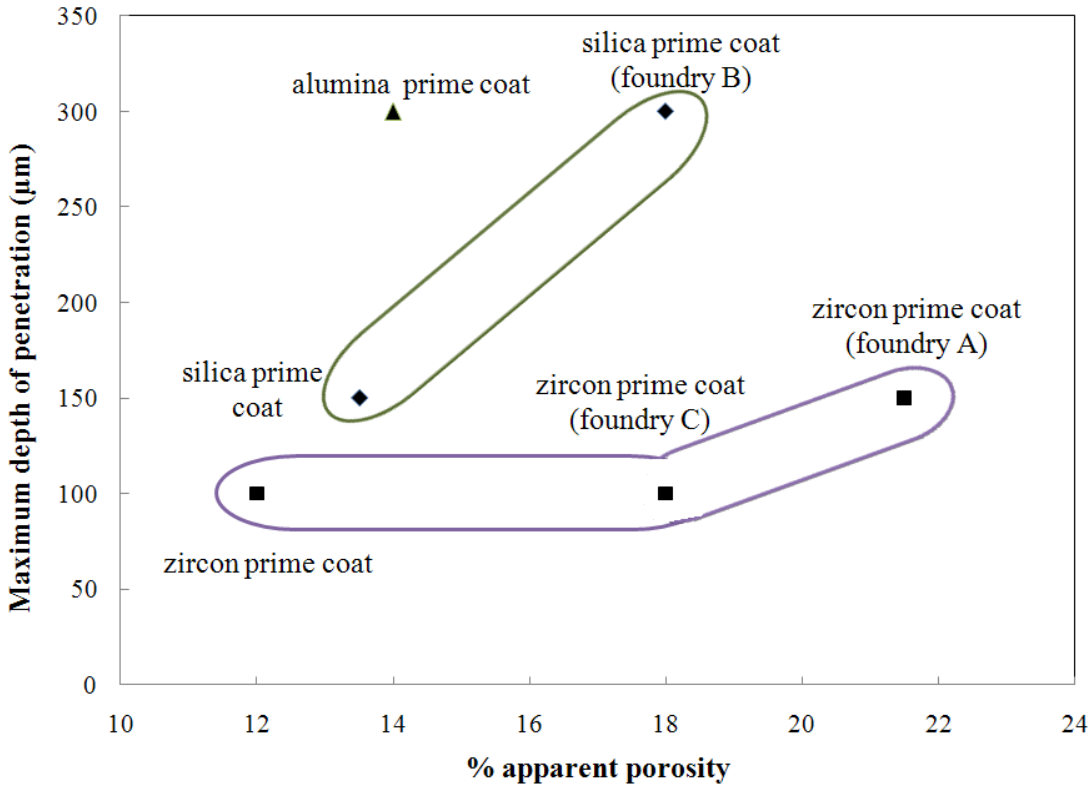

Figure 4.18 Maximum depth of reaction product location in prime coat of studied shell versus percentage apparent porosity

4.7. CONCLUSIONS

Metal-ceramic shell interaction products were studied in investment casting of low carbon alloy steel. *Al-Si-Mn-O* and *Fe-Si-Mn-O* were observed as the most common interaction products at the interface between shell and steel. Depth of the penetration depended on composition of the prime coat and the shell porosity at constant pouring temperature and the casting geometry. Shell with zircon in the prime coat had least amount of interaction products and less depth of reaction.

Thermodynamic prediction by Factsage and experimental results showed similar interaction products. The possible mechanism for liquid steel-ceramic shell interaction could be given as reaction of the reoxidation slag with the solid prime coat materials.

4.8. RECOMMENDATIONS

From the observations and conclusions found during the research following recommendations can be made.

1. Prevent re-oxidation

   Reduce exposure of the melt to atmospheric oxygen.

2. Use minimum superheat required to fill the shells completely.

   a. Superheat increases re-oxidation.

   b. Low superheat limits reaction time with the shell.

3. Use zircon as prime coat refractory.

4. Minimize deep pockets if possible in design.

4.9. AREAS OF FUTURE INTEREST

During this research it was observed that many parameters could be involved simultaneously affecting liquid steel – ceramic shell interactions in investment casting. Due to limited time and resources they were not explored in detail.

The following studies can be conducted to understand the interactions phenomenon.

4.9.1. Effect of superheat: The research conducted involved investment casting shells poured one after the other once desired superheat was achieved in the induction furnace. However, the same study can be done to evaluate effect of superheat. Similar shells can be poured with different superheats. Analysis of the interaction products and depth of penetration in prime coat can give better insight of the phenomenon.

4.9.2. Effect of inhibitor gas: An inert gas can be used to prevent liquid-steel ceramic shell interactions and its extent to reduce reactions can be determined. Furthermore, composition of the gas can be changed and similar analysis can be performed.

4.9.3. Vacuum induction melting: Investment casting shells with the same geometry can be poured in vacuum and the results can be compared with shells poured without vacuum.

Since there are many parameters involved and each can have considerable effect during on results shell composition and shell making procedure should be kept unchanged.

APPENDIX

Table 1. Thermal conductivities measured by different authors

Researcher	Method and Shell type	Temperature (°C)	Thermal Conductivity (W/mK)
Sabau,	Hot Wire and Laser FlashMethod	300	0.6
Viswanathan	Measured for 10 back up coats	750	0.8
	comprised of fused silica	1300	1.6
		1400	1.7
		1500	1.6
	Measured for Zircon prime coat	200	2.6
		300	2.4
		400	2.2
		500	2.1
		800	2
		900	2
		1000	1.9
		1100	1.9
Browne, Sayers	Thermal probe method	100	1.168
	Zircon slurry and Molochite	200	1.112
	16-30 stucco	300	1.128
		400	1.144
		500	1.086
		600	0.95
		700	1.326
Huang, Berry,	Hot Wire Method	100	0.3
Zheng, Piwonka	68% fused Silica + 32% zircon	200	0.32
		300	0.33
		400	0.35
		500	0.37
		600	0.38
		700	0.4
	85% fused silica + 15% alumina	100	0.31
		200	0.32
		300	0.34
		400	0.35
		500	0.36
		600	0.38
		700	0.39

Table 2. Specific heat capacities measured by different authors

Researcher	Method and Shell type	Tempearture (°C)	Specific Heat (J/KgK)
Browne, Sayers	Measured from thermal diffusivity	20	1365
	Zircon slurry and Molochite	1000	2239
	16-30 stucco		
Connolly, Jones,	Differential Scanning Calorimetry	300	1000
Marquis	Prima coat (silica + zircon based	400	1050
	slurry and molochite stucco)	500	1090
	Next 2 coats (silica based slurry	600	1100
	and molochite stucco)	700	1150
		750	1200
Sabau,	Hot Wire and Laser FlashMethod	150	1800
Viswanathan	Measured for Zircon prime coat	200	2000
		300	2200
		400	2250
		500	2400
		600	2500
		700	2600
		800	2700
		900	2800
		1000	2850
		1100	2900

Table 3. Thermal conductivity models for two phase mixtures

Name of the model	Equation of the Model
Eucken	$K_{mix} = \frac{K_c + 2P(1-K_c/K_d)/(2K_c/K_d+1)}{1-P(1-K_c/K_d)/(2K_c/K_d+1)}$
Kingery	$1/K_{mix} = (1-V_d)/K_c + V_d/K_d$
Parallel	$\frac{K_{mix}}{K_c} = (1-V_d) + V_d\frac{K_d}{K_c}$
Series	$\frac{K_{mix}}{K_c} = \frac{1}{(1-V_d)+V_d\frac{K_d}{K_c}}$
Russell	$\frac{K_{mix}}{K_c} = \frac{1-V_d^{2/3}+\frac{K_d}{K_c}V_d^{2/3}}{1-V_d^{2/3}+V_d+\frac{K_d}{K_c}(V_d^{2/3}-V_d)}$
Son Frey	$\frac{K_{mix}}{K_c} = \frac{1-V_d^{1/3}+V_d+\frac{K_d}{K_c}(V_d^{1/3}-V_d)}{1-V_d^{1/3}+\frac{K_d}{K_c}V_d^{1/3}}$
Rayleigh-Devries	$\frac{K_{mix}}{K_c} = 1-\frac{3V_d}{\left(\frac{2+K_d/K_c}{1-K_d/K_c}\right)+V_d-\alpha\left(\frac{1-K_d/K_c}{4/3+K_d/K_c}\right)V_d^{10/3}+\ldots}$

Table 3. (Continued)

Maxwell	$\frac{K_{mix}}{K_c} = \frac{\frac{K_d}{K_c} + 2 - 2V_d\left(1 - \frac{K_d}{K_c}\right)}{\frac{K_d}{K_c} + 2 + V_d\left(1 - \frac{K_d}{K_c}\right)}$
Bruggeman	$1 - V_d = \frac{\frac{K_{mix}}{K_c} - \frac{K_d}{K_c}}{\left(\frac{K_{mix}}{K_c}\right)^{1/3}\left(1 - \frac{K_d}{K_c}\right)}$

K_c = thermal conductivity of continuous phase

K_d = thermal conductivity of discontinuous phase

V_d = volume fraction of discontinuous phase

K_{mix} = thermal conductivity of the mixture

P = porosity

The themo- physical properties developed during the research are compiled here

Table 4. Density measurement for shells using Archimedes method

	Dry Weight (g)	Water Suspended (g)	Air Suspended (g)	% Open porosity	Bulk Density (g/cm3)
silica (silica prime coat)	12.20	6.31	13.13	13.64	1.79
silica + zircon	16.40	9.06	17.16	9.38	2.02
silica + aluminosilicate	9.60	5.29	10.33	14.48	1.90
alumina prime coat	11.20	5.63	11.97	12.15	1.77
zircon prime coat	10.70	5.45	11.56	14.08	1.75
foundry A	10.00	5.20	11.32	21.57	1.63
foundry B	11.60	7.00	12.60	17.86	2.07
foundry C	12.50	6.93	13.72	17.96	1.84

Properties of fused silica based investment casting shells by laser flash test

Table 5. Specific heat capacity and thermal conductivity

Temperature (°C)	Cp (J/KgK)	K (W/mK)
200	939	1.06
300	1047	1.18
400	1137	1.30
500	1210	1.41
600	1311	1.57
700	1428	1.76
800	1508	2.02
900	1560	2.37
1000	1730	2.81
1100	1811	3.37
1200	1807	4.14
1300	1807	4.14
1400	1807	4.14
1500	1807	4.14
1600	1807	4.14

Properties of zircon and fused silica based investment casting shells by laser flash test

Table 6. Specific heat capacity and thermal conductivity

Temperature (°C)	Cp (J/KgK)	K (W/mK)
200	745	1.01
300	823	1.08
400	907	1.19
500	985	1.30
600	1099	1.49
700	1198	1.67
800	1256	1.75
900	1410	2.14
1000	1551	2.48
1100	1517	3.13
1200	1551	3.64
1300	1551	3.64
1400	1551	3.64
1500	1551	3.64
1600	1551	3.64

Properties of fused silica and aluminosilicate based investment casting shells by laser flash test

Table 7. Specific heat capacity and thermal conductivity

Temperature (°C)	Cp (J/KgK)	K (W/mK)
200	792	0.86
300	898	0.94
400	1006	1.05
500	1091	1.14
600	1252	1.31
700	1368	1.49
800	1470	1.62
900	1622	1.85
1000	1996	2.32
1100	2187	2.66
1200	2383	3.22
1300	2382	3.22
1400	2382	3.22
1500	2382	3.22
1600	2382	3.22

BIBLIOGRAPHY

1. ASM Handbooks, Vol. 15 Castings, Investment Casting, Design Advantages of Investment Castings.
2. ASM Handbooks, Vol. 15 Castings, Investment Casting, Introduction.
3. Darryl Kline, Controlling Strength and Permeability of Silica Investment Casting Molds, Missouri University of Science and Technology, Thesis 2010, pp 26-27.
4. M.J. Hendricks, D.R. Engelhardt, Thermal Conductivity and Heat Transfer Measurement for Ceramic Shell Molds, 8th World Conference on Investment Casting, 28-30 June 1993, London Hilton, Vol. 2, paper # 11.
5. S. Lekakh, V. Richards, E. Druschitz, New Method of Dynamical Measurements of Mold Thermal Properties and Applications for Casting Processes, AFS Transactions © American Foundry Society, Schaumburg, IL, Paper 07-108(04), pp 1-7.
6. H. Huang, J.T. Berry, X.Z. Zheng, T.S. Piwonka, Thermal Conductivity of Investment Casting Ceramics, 37th Annual Technical Meeting : Investment Casting Institute 1989.
7. W.D. Kingery, M. Adams, A.L. Loeb, J. Frencl, R.L. Coble, T. Vasilos, M.C. McQuarrie, Thermal Conductivity, Journal of American Ceramic Society, Part II, Vol. 37, No. 2, Feb 1, 1954, pp 67-110.
8. D.J. Browne, K. Sayers, Simulation of Investment Casting – The Determination of Mould Thermo-physical Properties, 8th World Conference on Investment Casting, 28-30 June 1993, London Hilton, Vol. 2, Paper # 18.
9. S. Connolly, S.J ones, P.M. Marquis, Specific Heat of Investment Casting Shells, BICTA, April 2004, Issue 44, pp 23-26.

10. S. Sabau, S. Viswanathan, Thermo-physical Properties of Zircon and Fused Silica Based Shells for Investment Casting, Transactions of American Foundry Society, Vol. 112, Paper 04081, pp 649-661.
11. V.L. Richards, B. Kruse, Thermal and Moisture Characterization During Autoclave Dewaxing in Investment Casting, Proceedings of 59th SFSA T&O Conference, Paper 5.5, pp 1-39.
12. Transport phenomena in Materials Processing, Fourier's Law and Thermal conductivity of Materials, pp 208-215.
13. R.G. Gilliland, Silica Sand Transformations at Metal/Mold Interface During and After Solidification – A Preliminary Report, AFS Transactions, 1974, pp 301-308.
14. E. Brooks, C. Beckermann, V. L. Richards, Prediction of Burn on and Mold Penetration in Steel Casting Using Simulation, IJCM, Vol. 20, no 4, 2007.
15. V.L. Richards, Metal Penetration in Sand Molds: The Adherent Sand Defect, Steel Founder's Society of America Technical and Operating Conference, 1996.
16. V. L. Richards, Mold-Metal Penetration 2: More Adherent Sand Defects, Steel Founder's Society of America Technical and Operating Conference, November 6-8, 1997.
17. V. L. Richards, R. Monroe, Control of metal penetration in steel castings production, Steel Founder's Society of America Technical and Operating Conference, 1999.
18. V. L. Richards, D. Rasquinha, Burn In/ Burn On Case Study Findings, Steel Founder's Society of America Technical and Operating Conference, November, 2002.

19. V. L. Richards, S. Lekakh, B. Kruse, Burn In/Burn On: Coating characterization and Design Experiments, Steel Founder's Society of America Technical and Operating Conference, November 4-6, 2004, Paper 5.3.

20. K.D. Hayes, J.O. Barlow, D.M. Stefanescu, T.S. Piwonka, Mechanical penetration of Liquid Steel in Sand Molds, Transactions of the American Foundrymen's Society, V 106, Paper No 98-156, P 769-776, 1998.

21. K.D. Hayes, J.O. Barlow, D.M. Stefanescu, T.S. Piwonka, Chemical penetration of Liquid Steel in Sand Molds, Transactions of the American Foundrymen's Society, V 104, Paper No 97-145, P 325-331, 1997.

22. D.M. Stefanescu, M.D. Owens, A.M. Lane, T.S. Piwonka, K.D. Hayes, J.O. Barlow Penetration of Liquid Steel in Sand Molds, Part 1: Physics and Chemistry of Penetration and Mathematical Modeling-Metal Side, Transactions of the American Foundry Society, V 109, Paper No 01-058, P 1-17, 2001.

23. A.M. Lane, M.D. Owens, D.M. Stefanescu, T.S. Piwonka, J. O. Barlow, K.D. Hayes, Penetration of Liquid Steel in Sand Molds, Part 2: Chemical Reactions at the Mold/Metal Interface During Casting of Steel, Transactions of the American Foundry Society, V 109, Paper No 01-057, P 1-19, 2001.

24. K.D. Hayes, J.O. Barlow, D.M. Stefanescu, T.S. Piwonka, Penetration of Liquid Steel in Sand Molds, Part 3: Experimental Evaluation of the Metal-Molding Aggregate Interaction, Transactions of the American Foundry Society, V 109, Paper No 01-083, P 1-14, 2001.

25. G. A. Colligan, L. H. Van Vlack and R. A. Flinn, Factors affecting metal-mold reactions, AFS Transactions, Vol. 69, page 52-58, 1961.

26. K. Tani, Y. Ueda, S. Mori, Interfacial Reaction Between Cast Steel and Olivine Sand or Silica Sand, Transactions of the Iron and Steel Institute of Japan, Vol. 27, No. 3, Paper 197-2041987.
27. C. Cingi, J. Vainola, J. Orkas, Role of Oxygen in Mould-Metal Reactions in Investment Casting of Magnesium Alloy AZ91E, International Foundry Research, Vol. 59, No. 2, pp 18-27.
28. S. Jones, P.M. Marquis, B. Page, The Characterization of Thermal Profiles and Metal-Mold Interaction Within Investment Casting Moulds, Precast 93, Brno, Czech Republic, 17- 20 May 1993, pp 101-108.
29. Z. Zhang, G. Morin, Effect of Inhibitor Gas on Mould-Magnesium Reactions in Investment Casting, Magnesium Technology 2004, TMS Annual Meeting, Charlotte, NC, 14-18 March 2004, pp197-202.
30. S. Sikkenga, Gases in Air melt Investment Cast Alloys, Incast (USA), May 2001, Vol. 14, No. 4, pp 28-32.
31. K. Shinzato and T. Baba, A Laser Flash Apparatus for Thermal Conductivity and Specific Heat Capacity Measurements, Journal of Thermal Analysis and Calorimetry, Vol. 64 (2001) page 413-422.
32. Standard Test Method for Thermal Diffusivity by the Flash Method, ASTM E 1461-07.
33. James F. Shackelford, William Alexander, CRC Practical Handbook of Materials Selection, Page 404-415.
34. http://www.Quartzpage.de, Aug 25, 2010.

35. The Nomenclature of Silica, Gilbert Hart, American Mineralogist, Vol. 12, pages 383-395, 1927

36. V. L. Richards, S. Lekakh, D. Kline, C. Mahimkar, Crack formation in ceramic shell during foam pattern firing, SFSA T&O Conference, 2009

37. C. Mahimkar, V. L. Richards, S. Lekakh, High temperature thermo-physical properties of ceramic shell, Investment Casting Institute 57th Technical Conference & Expo, Oct 10-13, 2010.

38. Standard test methods for apparent porosity, water absorption, apparent specific gravity and bulk density of burned refractory brick and shapes by boiling water, ASTM C 20-00.

VITA

Chirag Mahimkar was born in Mumbai, India on June 2, 1986. In June 2002 he graduated from Parle Tilak Vidyalaya High School after completing his SSC. In June 2004 he graduated from Sathaye College finishing his HSC. Four years later, in June 2008 he received his B.E. degree in Chemical Engineering from D.J. Sanghvi College of Engineering affiliated to Mumbai University. In July 2011 he received a M.S. degree in Materials Science and Engineering from Missouri University of Science and Technology, Rolla, Missouri. During the Masters he was employed as research intern at ArcelorMittal, Global Research and Development, East Chicago.

Chirag has been a member of American Foundry Society since 2008 and Material Advantage since 2010. He has written two technical articles. The first one was "High Temperature Thermo-physical Properties of Ceramic Shells" published in Investment Casting Institute's 57th Annual Technical Conference and Expo. The second one was "Metal-Ceramic Shell Interactions During Investment Casting" for American Foundry Society's 115th Metalcasting Congress. In addition to authoring the technical articles, he has been co-author of two papers written by Dr. K. Chandrashekhara and one by Dr. Von Richards.